4. SITE 1076[1]

Shipboard Scientific Party[2]

HOLE 1076A

Position: 5°4.1316′S, 11°6.0917′E

Start hole: 2345 hr, 26 August 1997

End hole: 1830 hr, 27 August 1997

Time on hole: 18.75 hr

Seafloor (drill pipe measurement from rig floor, mbrf): 1415.7

Total depth (drill pipe measurement from rig floor, mbrf): 1620

Distance between rig floor and sea level (m): 11.5

Water depth (drill pipe measurement from sea level, m): 1404.2

Penetration (mbsf): 204.3

Coring totals:
Type: APC
Number: 22
Cored: 204.3 m
Recovered: 217.47 m (106.45%)

Lithology:
Unit I: organic carbon–rich olive-gray and greenish gray clay

HOLE 1076B

Position: 5°4.1344′S, 11°6.0922′E

Start hole: 1830 hr, 27 August 1997

End hole: 2255 hr, 27 August 1997

Time on hole: 4.42 hr

Seafloor (drill pipe measurement from rig floor, mbrf): 1413.6

Total depth (drill pipe measurement from rig floor, mbrf): 1474.5

Distance between rig floor and sea level (m): 11.5

Water depth (drill pipe measurement from sea level, m): 1402.1

Penetration (mbsf): 60.9

Coring totals:
Type: APC
Number: 7
Cored: 60.9 m
Recovered: 25.87 m (42.48%)

Lithology:
Unit I: organic carbon–rich olive-gray and greenish gray clay

HOLE 1076C

Position: 5°4.1309′S, 11°6.1048′E

Start hole: 2255 hr, 27 August 1997

End hole: 1155 hr, 28 August 1997

Time on hole: 13.00 hr

Seafloor (drill pipe measurement from rig floor, mbrf): 1413.9

Total depth (drill pipe measurement from rig floor, mbrf): 1617

Distance between rig floor and sea level (m): 11.5

Water depth (drill pipe measurement from sea level, m): 1402.4

Penetration (mbsf): 203.1

Coring totals:
Type: APC
Number: 22
Cored: 203.1 m
Recovered: 216.8 m (106.75%)

Lithology:
Unit I: organic carbon–rich olive-gray and greenish gray clay

HOLE 1076D

Position: 5°4.1312′S, 11°6.1150′E

Start hole: 1155 hr, 28 August 1997

End hole: 0215 hr, 29 August 1997

Time on hole: 14.33 hr

Seafloor (drill pipe measurement from rig floor, mbrf): 1412.5

Total depth (drill pipe measurement from rig floor, mbrf): 1526

Distance between rig floor and sea level (m): 11.5

Water depth (drill pipe measurement from sea level, m): 1401

Penetration (mbsf): 113.5

Coring totals:
Type: APC
Number: 12
Cored: 113.5 m
Recovered: 118.41 m (104.33%)

Lithology:
Unit I: organic carbon–rich olive-gray and greenish gray clay

Principal results: Site 1076 is the shallow-water drill site on a depth transect in the Lower Congo Basin. It is located in 1402 m deep water in a complex environment dominated by (1) freshwater input from the Congo River, (2) seasonal coastal upwelling and associated filaments and eddies moving offshore, and (3) incursions of open-ocean waters, especially from the South Equatorial Countercurrent. We expect a close tie-in of climatic records from the continent and the ocean in this area. In the fan-margin deposits, the intercalation of pelagic and terrigenous information provides an excellent opportunity for studying cross-correlations of climatic effects on land and at sea. Site 1076, in connection with Sites 1075 and 1077 in the Lower Congo Basin, will allow us to reconstruct the changing influence of Congo River, coastal upwelling, and open-ocean contributions to the dynamics of the region.

[1]Wefer, G., Berger, W.H., Richter, C., et al., 1998. *Proc. ODP, Init. Repts.,* 175: College Station, TX (Ocean Drilling Program).
[2]Shipboard Scientific Party is given in the list preceding the Table of Contents.

Four holes were cored with the advanced hydraulic piston corer (APC) at Site 1076 to a maximum depth of 204.3 meters below seafloor (mbsf), which recovered an apparently continuous hemipelagic sedimentary section spanning the last 1.5–1.6 m.y of the Pleistocene. Hole 1076A was cored with the APC to 204.3 mbsf. Seven APC cores were taken at Hole 1076B before the hole was abandoned because of lack of recovery. Hole 1076C was cored with the APC to 203.1 mbsf, and Hole 1076D to 113.5 mbsf.

The sediments form one lithostratigraphic unit composed of bioturbated organic carbon–rich olive-gray clay and greenish gray clay. Small shell fragments are present in many intervals. Above 150 mbsf, the calcium carbonate concentration alternates between 3 and 16 wt% and is limited below 150 mbsf to a maximum of 3.5 wt%. The biogenic portion of the sediment contains rare to abundant diatoms with rare nannofossils, silicoflagellates, siliceous sponge spicules, phytoliths, and traces of radiolarian and foraminifer fragments. Diatoms are abundant in both greenish gray and olive-gray intervals. Authigenic components are dominated by the presence of glauconite, dolomite, and iron sulfides. Rare, friable nodules, possibly phosphatic, are sometimes disseminated throughout certain intervals. Sedimentation rates vary between 250 m/m.y. in the uppermost 80 mbsf, 50 m/m.y. between 80 and 120 mbsf, and 210 m/m.y. between 120 and 200 mbsf.

Detailed comparisons between the magnetic susceptibility record generated on the multisensor track (MST) and the high-resolution color reflectance measured with the Minolta spectrophotometer demonstrated complete recovery of the sedimentary sequence down to 140 meters composite depth (mcd).

Calcareous microfossils show evidence of reworking. Their abundance and preservation deteriorates gradually between 100 and 200 mbsf. Siliceous microfossils are relatively abundant, well preserved, and show no evidence of reworking. The calcareous nannofossil-based biostratigraphy disagrees with the paleomagnetic time frame for the lower half-interval of Hole 1076A. We tentatively explain this discrepancy as a result of both poor preservation and reworking of calcareous nannofossils. Both calcareous nannofossil and benthic foraminiferal assemblages suggest a discontinuity within the sedimentary record at a depth of 120 mbsf. Downcore changes in planktonic foraminiferal and diatom assemblages are used as indices of variable surface and subsurface hydrography, as well as proxies for coastal upwelling and fluvial input.

A magnetostratigraphy was determined after alternating-field (AF) demagnetization at 20 mT. The Matuyama/Brunhes boundary occurs at ~138 mbsf, and the onset and termination of the Jaramillo Subchron (C1r.1n) was identified in the lower part of the section. A short reversal event in the Brunhes Chron (possibly the Blake event) occurs at all four holes.

Interstitial water profiles record the complete consumption of dissolved sulfate within the uppermost 20 mbsf. In this interval, alkalinity and ammonium also increase sharply, recording the degradation of organic matter. The distributions of dissolved strontium, calcium, and magnesium suggest two depth domains of carbonate dissolution and reprecipitation reactions: the first from 0 to 50 mbsf and the deeper from 120 to 200 mbsf.

The average concentration of total organic carbon (TOC) is 2 to 6 wt%, which is rather high for ocean margin areas and reflects a history of elevated primary production in this area. The organic matter appears to be mostly marine in origin. Its microbial degradation in the sediments has fueled a sequence of redox processes. One consequence of the degradation has been the production of moderate amounts of biogenic methane and carbon dioxide and additional dissolution of calcareous sediment components within the sediment.

Physical sediment properties were determined both by high-resolution MST core logging and index properties measurements. Magnetic susceptibility and gamma-ray attenuation porosity evaluator (GRAPE) signals reveal pronounced cyclicities, which were used for high-quality stratigraphic correlation in conjunction with digital color data.

Through its position within the domain of Congo River sedimentation and its high-resolution continuous record back through much of the Quaternary, Site 1076 will provide the basis for a tie-in of climatic records of west Africa, Congo River activity, coastal upwelling, and eastern tropical ocean dynamics. Of special interest are the competing source effects for land-derived materials, with some (most?) being brought directly by the river and the rest originating from reworked shelf sediments, especially during low sea-level periods.

BACKGROUND AND OBJECTIVES

For a discussion of the background and objectives for Site 1076, see "Background and Objectives" section, "Site 1075" chapter (this volume).

OPERATIONS

Hole 1076A (Proposed Site LCB-4)

The 64-nmi voyage from Site 1075 to Site 1076 was accomplished at an average speed of 11.4 kt. As the vessel slowly approached the location using Global Positioning System coordinates, the beacon was deployed at 2338 hr on 26 August. Hole 1076A was spudded at 0440 hr on 27 August. The seafloor depth was established at 1404.2 meters below sea level (mbsl) by drill-pipe measurement (DPM). APC Cores 175-1076-1H through 22H were taken from 0 to 204.3 mbsf (Table 1; also see expanded core summary table on CD-ROM, back pocket, this volume), with 204.3 m cored and 217.5 m recovered (106.3% recovery). Cores were oriented starting with 3H. The Adara heat-flow shoe was deployed at Cores 3H (23.8 mbsf), 5H (42.8 mbsf), 8H (71.3 mbsf), and 11H (99.8 mbsf). Headspace analysis of the cores indicates the presence of biogenic methane with minute amounts of ethane (<28 ppm) and no discernible amounts of heavier hydrocarbons. The methane concentration peaked at 66 mbsf (69,000 ppm) and gradually tapered off with depth. Although some of the cores exuded a mild sulphurous smell, concentrations of hydrogen sulfide were always <1 ppm and could not be measured. The drill string was pulled back with the bit clearing the seafloor at 1830 hr on 27 August, thereby ending Hole 1076A.

Hole 1076B

The vessel was offset 10 m to the east, and Hole 1076B was spudded at 1908 hr on 27 August. The seafloor depth was established at 1402.1 mbsl by DPM. After seven APC cores (0–60.9 mbsf), the hole was abandoned because virtually no sediment was recovered in Cores 175-1076B-5H, 6H, and 7H. The drill string was pulled out of the hole and cleared the seafloor at 2250 hr on 27 August, ending Hole 1076B.

Hole 1076C

The vessel was offset 20 m to the east, and Hole 1076C was spudded at 2325 hr on 27 August. APC Cores 175-1076C-1H through 22H were taken from 0 to 203.1 mbsf (Table 1), with 203.1 m cored and 216.8 m recovered (106.8% recovery). Cores were oriented starting with 4H. The drill string was pulled out of the hole with the bit clearing the seafloor at 1155 hr on 28 August.

Hole 1076D

The vessel was offset another 20 m to the east where the fourth and final hole of the site was spudded with the APC at 1230 hr on 28 August. The seafloor depth was established at 1401.0 mbsl by DPM.

Table 1. Coring summary for Site 1076.

Core	Date (Aug 1997)	Time (UTC)	Interval (mbsf)	Length cored (m)	Length recovered (m)	Recovery (%)
175-1076A-						
1H	27	0450	0.0-4.8	4.8	4.80	100.0
2H	27	0525	4.8-14.3	9.5	8.43	88.7
3H	27	0620	14.3-23.8	9.5	10.04	105.7
4H	27	0650	23.8-33.3	9.5	9.87	103.9
5H	27	0735	33.3-42.8	9.5	10.18	107.2
6H	27	0805	42.8-52.3	9.5	10.06	105.9
7H	27	0835	52.3-61.8	9.5	10.13	106.6
8H	27	0920	61.8-71.3	9.5	10.04	105.7
9H	27	0950	71.3-80.8	9.5	10.23	107.7
10H	27	1020	80.8-90.3	9.5	10.00	105.3
11H	27	1105	90.3-99.8	9.5	10.18	107.2
12H	27	1135	99.8-109.3	9.5	10.09	106.2
13H	27	1205	109.3-118.8	9.5	10.57	111.3
14H	27	1240	118.8-128.3	9.5	10.37	109.2
15H	27	1315	128.3-137.8	9.5	10.32	108.6
16H	27	1355	137.8-147.3	9.5	10.15	106.8
17H	27	1425	147.3-156.8	9.5	10.61	111.7
18H	27	1500	156.8-166.3	9.5	10.04	105.7
19H	27	1530	166.3-175.8	9.5	10.33	108.7
20H	27	1605	175.8-185.3	9.5	10.23	107.7
21H	27	1640	185.3-194.8	9.5	10.62	111.8
22H	27	1710	194.8-204.3	9.5	10.18	107.2
Coring totals:				204.3	217.47	106.5
175-1076B-						
1H	27	1915	0.0-3.9	3.9	3.90	100.0
2H	27	1945	3.9-13.4	9.5	10.15	106.8
3H	27	2010	13.4-22.9	9.5	9.83	103.5
4H	27	2045	22.9-32.4	9.5	1.73	18.2
5H	27	2115	32.4-41.9	9.5	0.26	2.7
6H	27	2145	41.9-51.4	9.5	0.00	0.0
7H	27	2215	51.4-60.9	9.5	0.00	0.0
Coring totals:				60.9	25.87	42.5
175-1076C-						
1H	27	2335	0.0-3.6	3.6	3.64	101.1
2H	28	0000	3.6-13.1	9.5	8.98	94.5
3H	28	0020	13.1-22.6	9.5	9.86	103.8
4H	28	0100	22.6-32.1	9.5	10.01	105.4
5H	28	0130	32.1-41.6	9.5	9.98	105.1
6H	28	0200	41.6-51.1	9.5	10.01	105.4
7H	28	0235	51.1-60.6	9.5	9.93	104.5
8H	28	0340	60.6-70.1	9.5	10.14	106.7
9H	28	0415	70.1-79.6	9.5	10.07	106.0
10H	28	0445	79.6-89.1	9.5	10.20	107.4
11H	28	0515	89.1-98.6	9.5	10.13	106.6
12H	28	0550	98.6-108.1	9.5	10.16	106.9
13H	28	0620	108.1-117.6	9.5	10.23	107.7
14H	28	0645	117.6-127.1	9.5	10.44	109.9
15H	28	0715	127.1-136.6	9.5	10.38	109.3
16H	28	0745	136.6-146.1	9.5	10.38	109.3
17H	28	0815	146.1-155.6	9.5	10.36	109.1
18H	28	0845	155.6-165.1	9.5	10.57	111.3
19H	28	0915	165.1-174.6	9.5	10.27	108.1
20H	28	0945	174.6-184.1	9.5	10.81	113.8
21H	28	1020	184.1-193.6	9.5	10.02	105.5
22H	28	1050	193.6-203.1	9.5	10.23	107.7
Coring totals:				203.1	216.80	106.8
175-1076D-						
1H	28	1245	0.0-9.0	9.0	9.00	100.0
2H	28	1315	9.0-18.5	9.5	9.96	104.8
3H	28	1350	18.5-28.0	9.5	9.93	104.5
4H	28	1420	28.0-37.5	9.5	10.05	105.8
5H	28	1450	37.5-47.0	9.5	10.04	105.7
6H	28	1520	47.0-56.5	9.5	10.03	105.6
7H	28	1555	56.5-66.0	9.5	10.10	106.3
8H	28	1625	66.0-75.5	9.5	8.69	91.5
9H	28	1720	75.5-85.0	9.5	10.17	107.1
10H	28	1755	85.0-94.5	9.5	10.11	106.4
11H	28	1825	94.5-104.0	9.5	10.12	106.5
12H	28	2210	104.0-113.5	9.5	10.21	107.5
Coring totals:				113.5	118.41	104.3

Notes: UTC = Universal Time Coordinated. An expanded version of this coring summary table that includes lengths and depths of sections and comments on sampling is included on CD-ROM (back pocket, this volume).

APC Cores 175-1076D-1H through 12H were taken from 0 to 113.5 mbsf (Table 1), with 113.5 m recovered (104.3%). The hole was aborted before the initial depth objective because of time constraints. The bit cleared the seafloor at 2030 hr on 28 August. While the drill string was being pulled out of the hole, the hydrophones and thrusters were retracted and secured, and the beacon was released and recovered at 2100 hr on 29 August, thereby ending operations at Site 1076.

SITE GEOPHYSICS

For a discussion of site geophysics at Site 1076, see "Site Geophysics" section, "Site 1075" chapter (this volume).

LITHOSTRATIGRAPHY

Introduction

Three holes with a maximum penetration of 205 mbsf were drilled at Site 1076 (Fig. 1). The upper 30 cm of the first five cores at all three holes were very disturbed and soupy and unsuitable for sampling. Severe core disturbances and large voids from gas release and core cutting of friable sediments occurred at the top and bottom sections of Cores 175-1076A-9H through 22H and 175-1076C-9H through 22H.

Description of Lithostratigraphic Unit

The lithostratigraphic description for the sedimentary sequence from Site 1076 is based on data from the following sources: (1) visual core description, (2) smear-slide examination, (3) color reflectance measurements, (4) bulk calcium carbonate measurements, and (5) X-ray diffraction (XRD) measurements.

Sediments from Site 1076 form one lithostratigraphic unit composed of organic carbon–rich olive-gray (5Y 3/2) to greenish gray (5GY 5/1) clay. The variation in color between olive-gray and greenish gray intervals may result from variations in several parameters: (1) organic carbon contents, (2) the relative contribution of the clay vs. the biogenic component, and (3) changes in the abundances of glauconitic clays and pyrite. Most of the sediments are bioturbated, which is most clearly seen in intervals with a pronounced change in sediment color. The clays progressively become more friable with depth as a result of compaction. Many cores contain gas expansion voids that were produced by the release of carbon dioxide trapped in the sediment (see "Organic Geochemistry" section, this chapter). A 3-cm-thick package of interlayered laminae of shell fragments and olive-gray clay is present in interval 175-1076C-14H-5, 45–47 cm. Laminae range in thickness from 2 to 3 mm. Shell-rich laminae are composed of broken pteropod shells and are discontinuous. The package has sharp lower and upper contacts (Fig. 2) and is coincident with the paraconformity described in the "Biostratigraphy and Sedimentation Rates" section (this chapter). In addition, small shell fragments are present in many intervals throughout the sediment recovered from this site. Above 150 mbsf, calcium carbonate in sediments alternates from a low of ~3 wt% to a maximum of 16 wt%. Below 150 mbsf, calcium carbonate preservation is poor and values are limited to a maximum of 3.5 wt%.

Synthesis of Smear-Slide Analyses

Smear-slide analyses indicate that the clastic component is dominated by clay minerals and minor amounts of quartz and feldspar. The biogenic portions of sediments contain rare to abundant diatoms with rare nannofossils, silicoflagellates, siliceous sponge spicules, phytoliths, and traces of radiolarian and foraminifer fragments. Diatoms

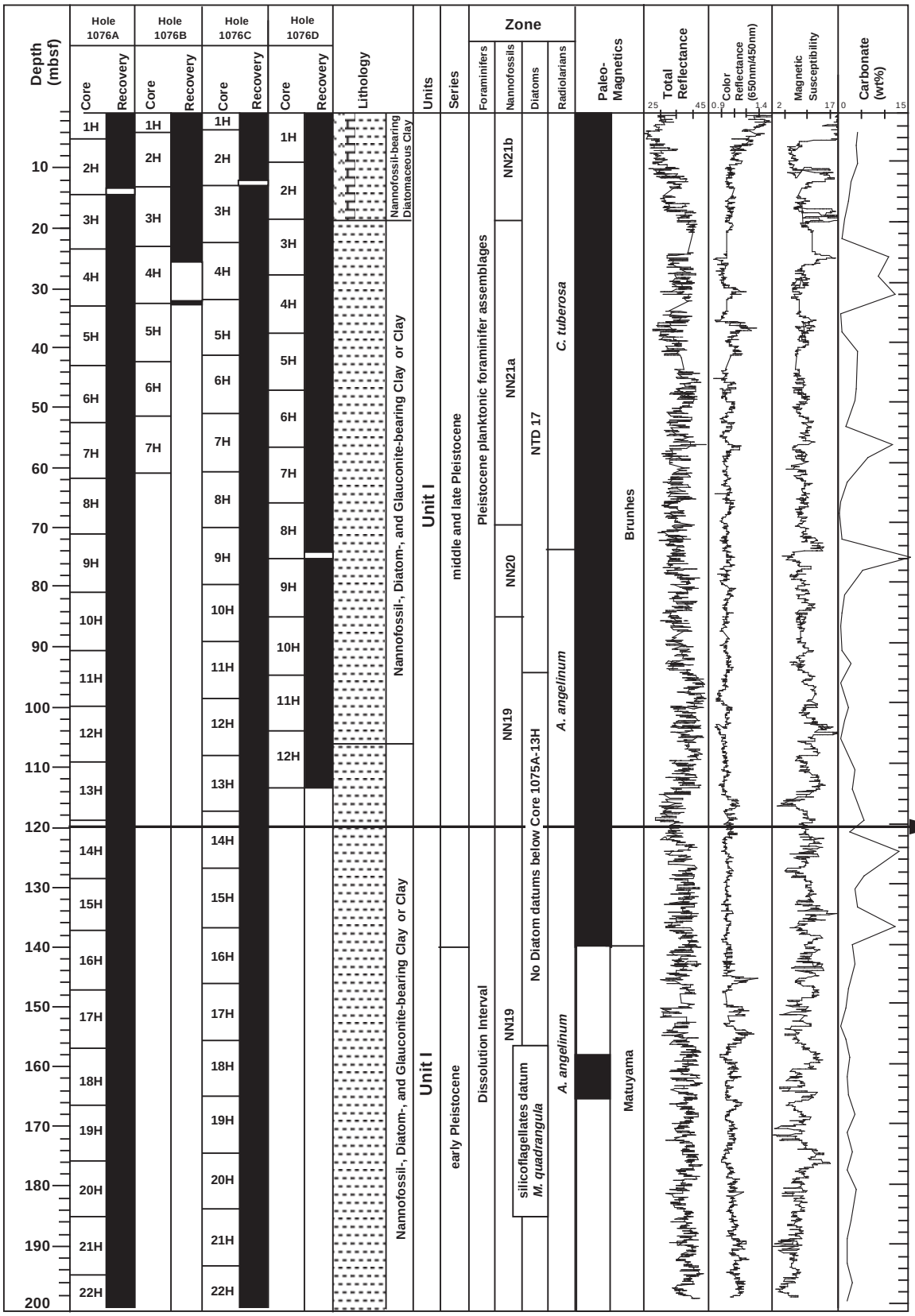

Figure 1. Composite stratigraphic section for Site 1076 showing core recovery in all holes, a simplified summary of lithology, age, total reflectance, color reflectance (650 nm/450 nm), magnetic susceptibility, and calcium carbonate content.

are abundant in both greenish gray and olive-gray intervals independently of organic carbon contents.

Authigenic components are dominated by the presence of glauconite, dolomite, and iron sulfides. Glauconite peloids, along with pyritized–worm casts, -diatoms and -radiolarians, are observed. Small dolomite rhombohedrons (6–100 µm) exist throughout. Iron sulfides are present primarily in the form of disseminated pyrite and framboidal pyrite, confirming the process of bacterial sulfate reduction. Rare, friable nodules, possibly phosphatic, are disseminated throughout certain intervals. Nodules range in diameter from 1 to 2 mm.

X-ray Diffraction Analysis

The XRD patterns of Hole 1076A document five major minerals: smectite, kaolinite/illite, quartz, calcite, and pyrite. The smectites are generally poorly crystallized. Shipboard XRD spectra for Site 1076 are not precise enough to determine the smectite crystallinity. The clay-mineral association in the Congo Basin area is controlled mainly by the varying contribution of these poorly crystallized smectites (van der Gaast and Jansen, 1984). As at Hole 1075A, low measured smectite values may represent large contributions of this mineral to the mineral association at this hole.

Comparison of the K/(K+Sm) ratios with the original kaolinite and smectite intensities shows that the peaks in the ratio represent high kaolinite counts that are not diluted by large amounts of low-crystalline smectite (Fig. 3). There is only one clear exception: at 96.5 mbsf, high kaolinite intensity coincides with high smectite intensity. Because kaolinite is a known product of chemical weathering of igneous rocks in the tropical rain forest (Singer, 1984) the high ratios, except the one at 96.5 mbsf, suggest humid periods in the Congo drainage area, whereas the lower ratios represent more arid periods.

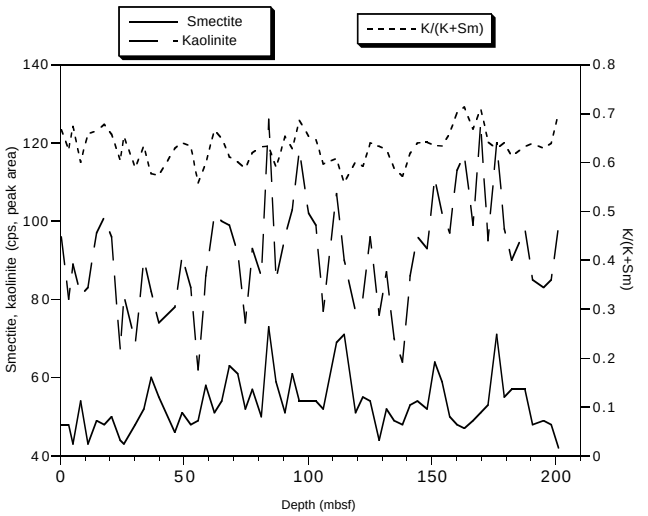

Figure 3. Stratigraphic variation in the ratio of smectite (Sm) to kaolinite (K), expressed as K/(Sm+K). Cps = counts per second.

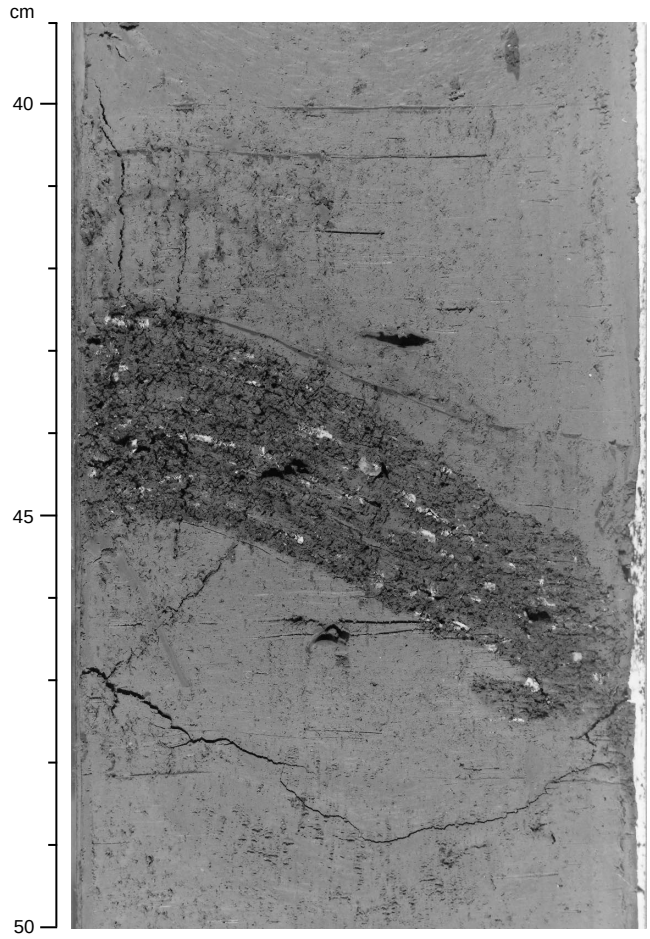

Figure 2. Interlaminated clay and pteropod-rich shell layers in interval 175-1076C-14H-5, 39–50 cm.

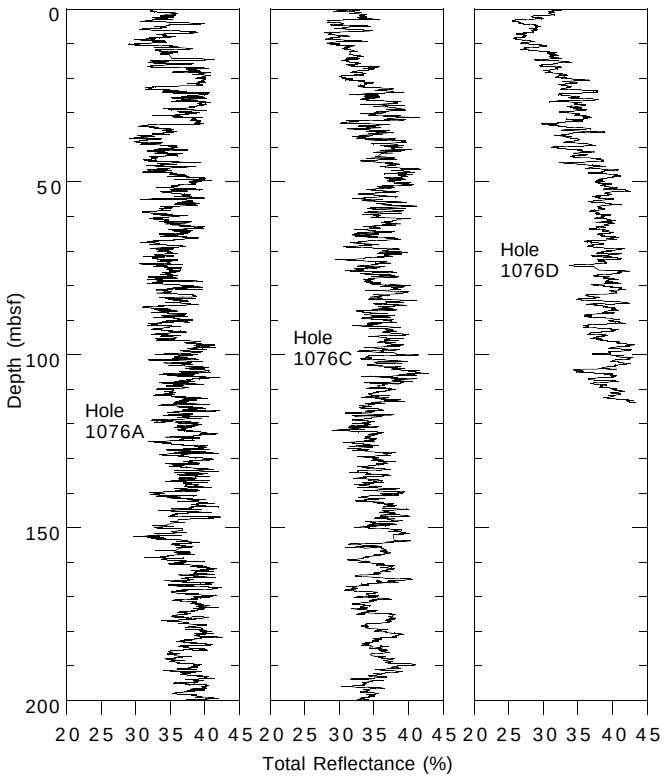

Figure 4. Stratigraphic variation in the total light reflectance for Holes 1076A, 1076C, and 1076D. Data have been smoothed over nine points for Hole 1076A and over five points for Holes 1076C and 1076D.

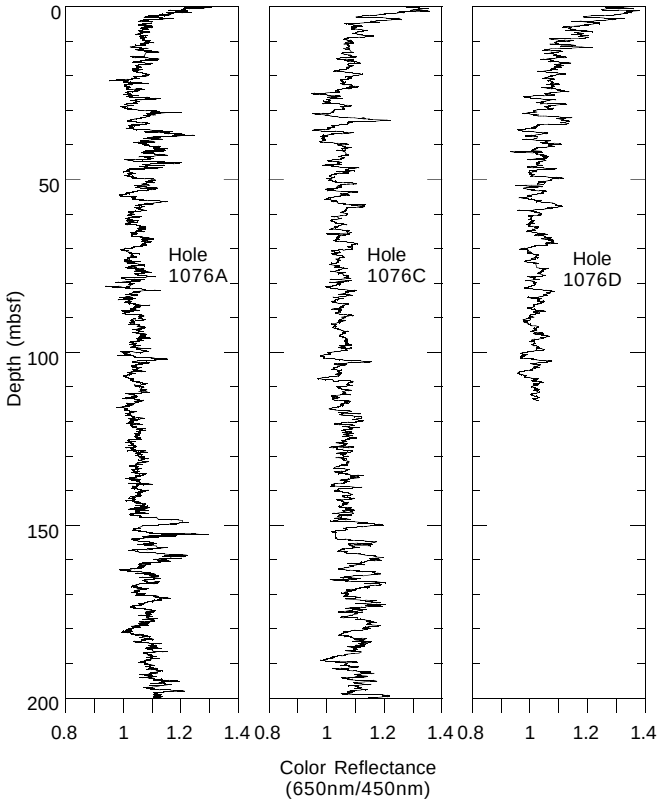

Figure 5. Stratigraphic variation in the ratio of the red (650 nm) to blue (450 nm) wavelengths at Holes 1076A, 1076C, and 1076D, displaying a pronounced periodicity possibly corresponding to the 23-k.y. precession cycle. Data have been smoothed over nine points for Hole 1076A and over five points for Holes 1076C and 1076D.

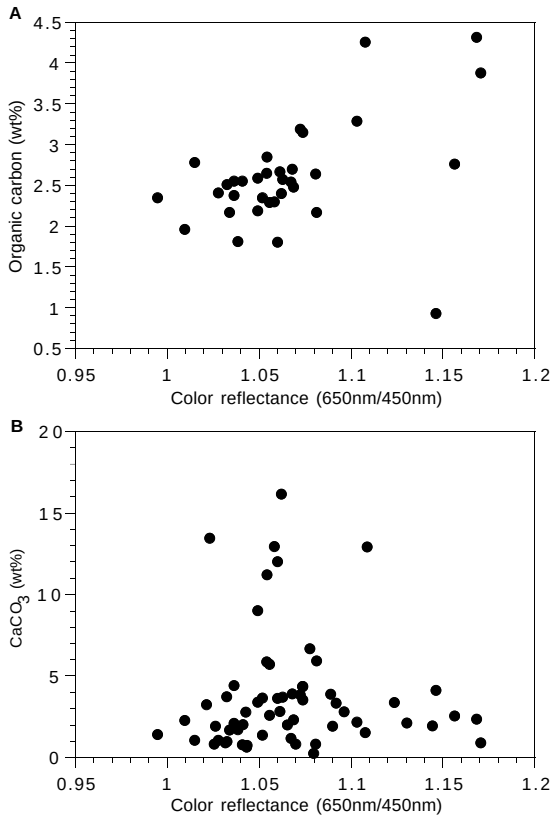

Figure 6. Relationship between the red/blue wavelength spectral ratio and the concentrations of (**A**) organic carbon and (**B**) calcium carbonate at Hole 1076A.

Spectrophotometry

Color data were measured every 2 cm for Hole 1076A. Holes 1076C and 1076D were measured at 4-cm intervals. The light reflectance data are in the range of 30% to 45% throughout the column recovered from Site 1076. The total reflectance (Fig. 4) and red/blue (650 nm/450 nm) ratio (Fig. 5) were smoothed over nine points for Hole 1076A and over five points for Holes 1076C and 1076D to remove smaller scale variability. Light reflectance records for Hole 1076A show marked intervals with higher reflectance values. The significance of these intervals is not readily apparent. Presumably, clay-rich sediments have a lower total reflectance (Mix et al., 1992), while carbonate-rich and diatom-rich sediments are more highly reflective. Thus, a high proportion of biogenous components may be indicated. The red/blue ratio presents no correlation with calcium carbonate and shows a weak correlation with organic carbon (see Fig. 6). Using the age model provided by the "Biostratigraphy and Sedimentation Rates" and "Paleomagnetism" sections (this chapter; see Fig. 1), periodicity in the red/blue ratio seems to be dominated by the 23-k.y. period.

BIOSTRATIGRAPHY AND SEDIMENTATION RATES

Sediment recovered from Site 1076 represents a relatively continuous hemipelagic section spanning the last 1.5–1.6 m.y. of the Pleistocene. The micropaleontological study was carried out on core-catcher samples from Hole 1076A. Additional samples from within the cores were examined for calcareous nannofossil- and silicoflagellate-based biostratigraphy.

Calcareous microfossil abundance and preservation deteriorates gradually from Core 175-1076A-11H through 22H. All three calcareous groups show evidence for common reworking in the majority of the samples. In contrast, siliceous microfossil are abundant and well preserved throughout Hole 1076A. The calcareous nannofossil-based biostratigraphy disagrees with the paleomagnetic time frame for the lower half of Hole 1076A. We tentatively explain this discrepancy as a result of both poor preservation and reworking of calcareous nannofossils.

Both calcareous nannofossil and benthic foraminiferal assemblages suggest a discontinuity within the sedimentary record at an approximate depth of 120 mbsf. Downcore changes in planktonic foraminiferal and diatom assemblages are used as indices of variable surface and subsurface hydrography, as well as proxies of coastal upwelling and fluvial input.

Calcareous Nannofossils

Nannofossil-derived biostratigraphy of Site 1076 is based on a high-resolution study of Hole 1076A. Table 2 indicates that most locations of datum events at Hole 1076A were constrained within a maximum range of 8 m. Because of frequent occurrences of calcareous nannofossil-barren samples toward the bottom part of Hole 1076A, there is a broader depth range (~11 m) in which the oldest datum (last occurrence [LO] of *Helicosphaera sellii*) can occur.

Nannofossil assemblages are generally characterized by low diversity and moderate to poor preservation. Reworked specimens are common throughout the entire section. The overall abundance ranges

Table 2. Microfossil datums at Hole 1076A.

Fossil group	Event	Age (Ma)	Zone (base) A	Zone (base) B	Core, section, interval (cm) Top	Core, section, interval (cm) Bottom	Depth (mbsf) Top	Depth (mbsf) Bottom	Depth (mbsf) Mean
					176-1076A-	176-1076A-			
N	FO *Emiliania huxleyi* acme	0.09	NN21b		3H-1, 80	3H-4, 60	15.10	19.40	17.3
N	FO *Emiliania huxleyi*	0.26	NN21a	CN15	8H-5, 30	8H-CC	68.15	71.84	70.0
N	LO *Gephyrocapsa caribbeanica* acme	0.26	NN21a	CN15	8H-5, 30	8H-CC	68.15	71.84	70.0
N	LO *Pseudoemiliania lacunosa*	0.46	NN20	CN14b	9H-CC	10H-5, 34	81.51	87.04	84.3
R	LO *Axoprunum angelinum*	0.46			8H-CC	9H-CC	71.84	81.51	76.7
N	LO Small *Gephyrocapsa* acme (Weaver, 1993)	0.60*			10H-CC	11H-3, 14	90.89	93.44	92.2
S	LO *Bachmannocena quadrangula*	0.80			16H-CC	17H-CC	147.90	157.86	152.9
N	LO *Reticulofenestra asanoi*	0.83			12H-2, 10	12H-4, 10	101.40	104.40	102.9
N	LO Small *Gephyrocapsa* acme (Gartner, 1977) Paraconformity	0.96		CN14a	13H-3, 50	13H-CC	111.70	119.85	115.8
N	LO Small *Gephyrocapsa* acme (Gartner, 1977)	0.96		CN14a	14H-6, 3	14H-CC	126.30	129.12	127.7
N	LO *Helicosphaera sellii*	1.25			20H-CC	21H-7, 10	185.98	196.34	191.2

Notes: Fossil group: N = calcareous nannofossils; S = silicoflagellates; and R = radiolarians. FO = first occurrence and LO = last occurrence. * = lower isotopic Stage 15 (Weaver, 1993); age interpolated from Imbrie et al. (1984). Zonal codes refer to the standard calcareous nannofossil zonations of (A) Martini (1971) and (B) Okada and Bukry (1980).

from abundant for Cores 175-1076A-1H through 10H and within Cores 175-1076A-13H and 14H, to poor or barren for Cores 175-1076A-11H and 12H and from Cores 175-1076A-15H through 22H.

The nannofossil biostratigraphy suggests that drilling at Site 1076 recovered a continuous stratigraphic record from the lower Pleistocene (lower part of Zone NN19) to the Holocene (upper Zone NN21b). Based on the identification of the LO of *H. sellii* datum near the base of Hole 1076A, the oldest sediment recovered from Site 1076 has an approximate age of 1.3 Ma.

The biostratigraphic framework disagrees with the paleomagnetic interpretations from 90 to 120 mbsf. Sedimentation rates calculated from nannofossil datums are lower than those estimated from paleomagnetic boundary events (Fig. 7). Reasons for this discrepancy probably include poor preservation and frequent reworking of nannofossil assemblages within Cores 175-1076A-11H and 12H, which affect primarily the LO datum events of individual species (i.e., LO of *Pseudoemiliania lacunosa* and LO of *Reticulofenestra asanoi*). However, we do not believe that the depth locations of datum events based on acme intervals (LO of Small *Gephyrocapsa* acme [sen. str. Weaver, 1993]; LO of Small *Gephyrocapsa* acme [sen. str. Gartner, 1977]) are affected by poor preservation or common reworked specimens. In any case, nannofossil-based estimates of sedimentation rates should be taken with extreme caution.

A major paraconformity was identified within the top part of Core 175-1076A-14H. This feature (see "Lithostratigraphy" section, this chapter) has the effect of duplicating similar nannofossil assemblage successions and datums above and below ~120 mbsf.

Zone NN21b

The uppermost three cores down to the mean depth of 17.3 mbsf (Sample 175-1076-3H-1, 80 cm, to Sample 175-1076-3H-4, 60 cm) are ranged within Zone NN21b. Nannofossil assemblages within this interval are dominated by *Emiliania huxleyi.*

Zone NN21a

Most of this interval ranges within the *Gephyrocapsa aperta* acme Zone sen. str. Weaver (1993) and extends throughout isotope Stages 6, 7, and upper 8. The lower boundary marker for Zone NN21a was identified within Core 175-1076A-8H at a mean depth of 70 mbsf.

Zone NN20

The LO *P. lacunosa* event (which marks the lowermost boundary of this zone) was difficult to constrain because of frequent reworking within Cores 175-1076A-9H and 10H. We tentatively located this event between Samples 175-1076A-9H-CC and 10H-5, 34 cm.

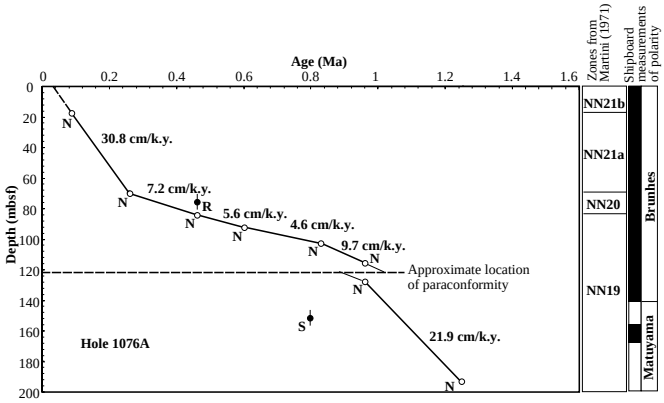

Figure 7. Age-depth plot and sedimentation rates at Hole 1076A estimated from calcareous microfossils (open circles; N = calcareous nannofossils) and siliceous microfossils (closed circles; S = silicoflagellates and R = radiolarians).

Zone NN19

Site 1076 did not penetrate the Zone NN19/NN18 boundary (uppermost Pliocene) but terminated slightly below the LO *H. sellii* datum event (Samples 175-1076A-20H-CC to 21H-7, 10 cm). Other datums identified within the Zone NN19 interval were the LO of *R. asanoi* at 102.9 mbsf and the LO of Small *Gephyrocapsa* acme sen. str. Gartner (1977) at both 115.8 and 127.7 mbsf (see above discussion on paraconformity).

Planktonic Foraminifers

The planktonic foraminifers at Site 1076 are affected by dissolution. In addition, there is evidence for reworking in the uppermost sample. One specimen of *Globorotalia tosaensis* (LO at 0.65 Ma) was identified in Sample 175-1076A-1H-CC. It is not present in the underlying samples and agrees with calcareous nannofossil floral distributions that indicate reworking.

Zonation schemes based on faunal changes within the Pleistocene (e.g., *Globorotalia menardii* and *G. truncatulinoides* zonations based on the presence/absence and the coiling direction, respectively) are not readily applicable because of dissolution and the broad sampling interval (core catchers).

The uppermost assemblage is dominated in the coarse fraction (>250 µm) by *Orbulina universa* (Fig. 8). Table 3 lists the dominant species for Site 1076 by decreasing susceptibility to dissolution. *Glo-*

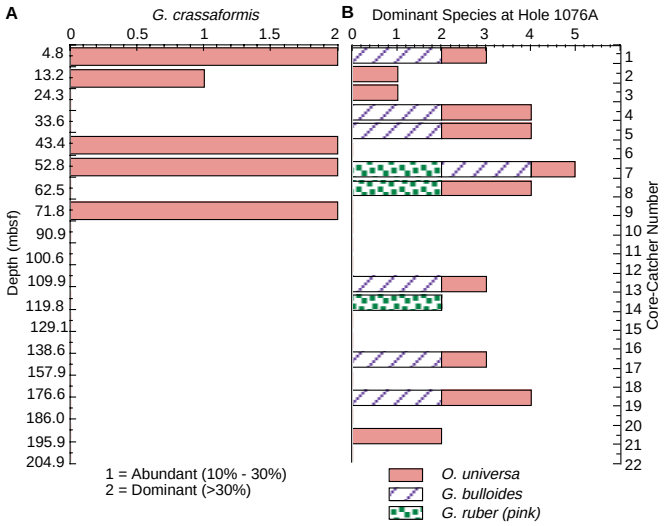

Figure 8. Planktonic foraminiferal abundances. **A.** Intervals where *G. crassaformis* is a dominant component of the assemblage. **B.** High abundances of *O. universa* and *G. bulloides* suggest modern conditions, whereas increased abundances of *G. ruber* (pink) indicate warm water or enhanced preservation or both. Abundance index: 5 = very abundant, 4 = abundant, 3 = common, 2 = few, 1= rare, and 0 = barren.

Table 3. The dominant and abundant planktonic foraminiferal species at Hole 1076A.

Core, section, interval	Dissolution intervals	*Globigerinoides ruber* (pink)	*Globigerinoides ruber*	*Orbulina universa*	*Globigerinoides sacculifer*	*Globigerina bulloides*	*Globigerinella siphonifera*	*Globorotalia inflata*	*Globorotalia menardii*	*Neogloboquadrina dutertrei*	*Neogloboquadrina pachyderma* (dextral)	*Globorotalia crassaformis*
175-1076A-												
1H-CC				D		A						A
2H-CC				D								D
3H-CC			A	D			A			A		
4H-CC			D	A		A				D	A	
5H-CC				A		A		A				A
6H-CC			A									A
7H-CC		A		D		A					A	
8H-CC		A		A							A	A
10H-CC	DISS											
11H-CC	DISS											
12H-CC			A							A	A	
13H-CC				A		A					D	
14H-CC		A	D		A						A	
15H-CC	DISS											
16H-CC	DISS											
17H-CC				A		A	A					
18H-CC												
19H-CC			A	A		A		A			A	
20H-CC	DISS											
21H-CC				D	A				D		A	
22H-CC	DISS											

Notes: Species listed in decreasing susceptibility to dissolution, from left to right. The positions of *H. siphonifera* and *G. quadrilobatus* have not been determined. A = abundant (10%–30%); D = dominant (>30%); DISS = barren or very few specimens (dissolution interval).

bigerina bulloides and *Globorotalia crassaformis* are abundant components. Other common species include *Neogloboquadrina pachyderma* (sinistral and dextral), *Globorotalia inflata*, and *G. scitula*. This assemblage differs from the uppermost assemblage at Site 1075 in that *Globigerinoides ruber* (pink) is not abundant. *O. universa* has been found in very high abundances south of the study area, in the Benguela Current region (Bé and Tolderlund, 1971), but it was not found in high abundances in a study performed in the Congo Basin (Ufkes et al., in press). The high abundance of *O. universa* (Fig. 8), in conjunction with the low abundance of *G. ruber* (pink), may be representative of the surface-water conditions at the eastern edge of the gyre. The dominance of *O. universa* and absence of *G. ruber* (pink) occurs in Samples 175-1076A-1H-CC through 5H-CC, as well as in Samples 175-1076A-13H-CC, 17H-CC, 19H-CC, and 21H-CC. The absence of *G. ruber* (pink) in these samples may be the result of dissolution, however, and be unrelated to surface-water changes.

G. crassaformis is abundant in the upper part of the section but is absent below Core 175-1076A-8H-CC (71.84 mbsf). Although these samples are within the dissolution interval (Samples 175-1076A-10H-CC through 22H-CC), dissolution-susceptible species such as *G. ruber* are present, suggesting that the absence of *G. crassaformis* may be related to a hydrographic change and not just to dissolution. *G. crassaformis* is commonly found at depths >100 m in this region, in the oxygen minimum zone, and below the Equatorial Undercurrent (Bé and Tolderlund, 1971).

The presence of *G. bulloides* presumably indicates elevated productivity, possibly related to upwelling. The consistent downcore presence of both *G. bulloides* and *O. universa* suggests that conditions similar to modern ones prevailed downcore in Samples 175-1076A-1H-CC, 4H-CC, 5H-CC, 7H-CC, 13H-CC, 17H-CC, and 19H-CC.

Benthic Foraminifers

The upper 10 core-catcher samples of Hole 1076A (Samples 175-1076A-1H-CC through 10H-CC) contain well-preserved benthic foraminifers in relatively high abundance. Farther downcore, the abundance is lower and the preservation moderate to poor. The preservation displays a dual character in the interval 175-1076A-13H-CC through 14H-CC (perhaps down to Sample 175-1076A-16H-CC, but the abundance of benthic foraminifers in those samples is very low). Here well-preserved specimens of *Hoeglundina elegans* are present with heavily eroded specimens of the same species. The upper part of that interval is equivalent with the "paraconformity," as suggested by the calcareous nannofossil assemblages.

The diversity of benthic foraminifers deteriorates downcore as a result of lower absolute abundance. This impedes a relevant analysis of faunal changes through time, even though some general comments can be made. *Bulimina aculeata* is continuously present in high relative abundance throughout Hole 1076A. Its presence is associated with high relative abundance of *B. exilis* and *Uvigerina auberiana.* Other species that are present in high relative abundance throughout Hole 1076A are *Bulimina mexicana, Cassidulina laevigata, Cibicidoides pachyderma,* fissurids, and the *Praeglobobulimina/Globobulimina* group (Fig. 9). The species *Epistominella* sp. 1 and *Quadrimorphina allomorphoides* are restricted to the upper part of Hole 1075A, whereas *Stilostomella* spp. occurs in the lower part only. Relative abundances of the benthic foraminiferal species found at Hole 1076A are presented in Table 4.

Most of the benthic foraminiferal species found at Site 1076 (Table 4) are long-ranging, cosmopolitan species that have been reported from the southeastern South Atlantic (Boersma, 1984a, 1986b). The faunal composition is indicative of upwelling and enhanced productivity; important species such as *Bulimina aculeata*

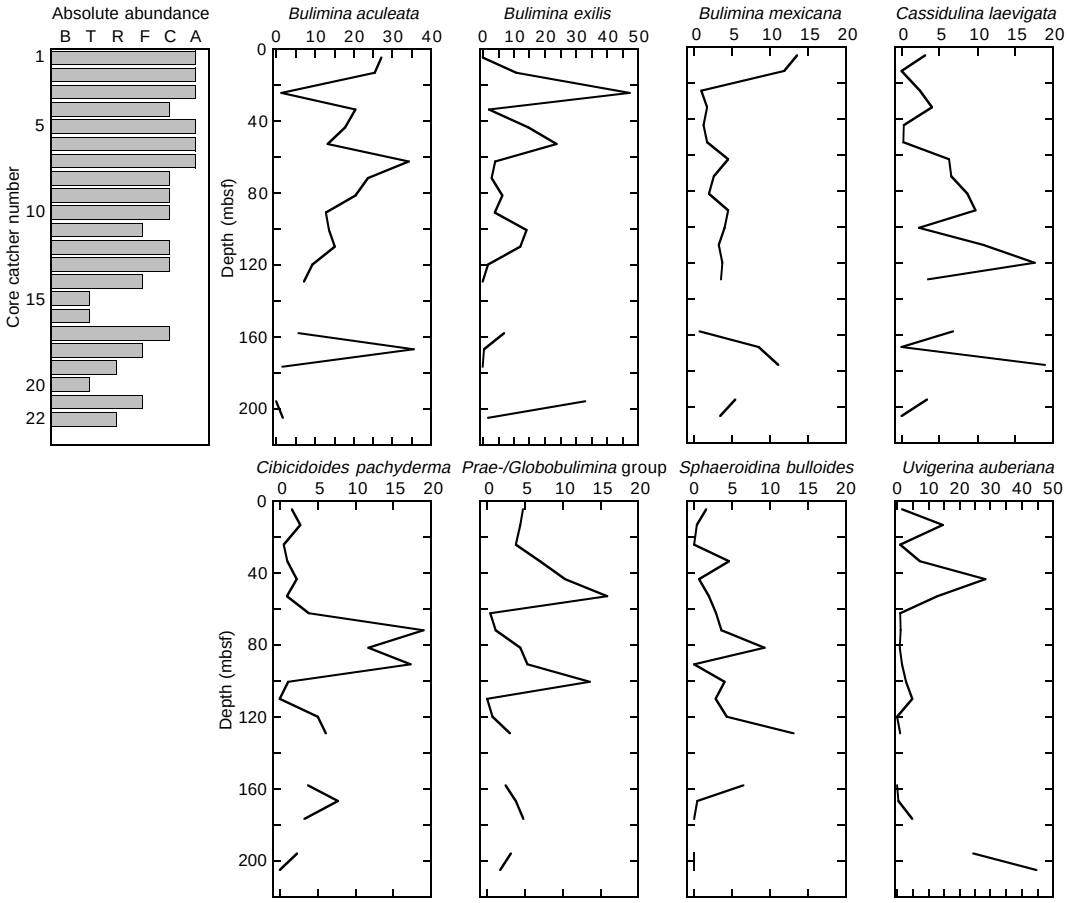

Figure 9. Relative abundances for selected benthic foraminiferal species. Absolute abundance (per ~20 cm^3 of sediment) of benthic foraminifers is given as A = abundant (>500 specimens); C = common (250–500 specimens); F = few (100–249 specimens); R = rare (50–99 specimens); T = trace (1–49 specimens); and B = barren (no specimens). Note that very few specimens were found in Samples 1076A-15H-CC, 16H-CC, and 20H-CC and that no reliable percentage estimates could be obtained.

and *B. exilis* are both reported to prefer such conditions. The species *B. aculeata* is reported to have high tolerance to oxygen deficiency and to prefer high nutrient abundance (Van der Zwaan, 1982); *B. exilis* is often associated with sapropels and diatomites formed under conditions of significant oxygen depletion (Jonkers, 1984). The species *B. mexicana* is present in high relative abundances at Hole 1076A, and it is reported to be common in regions of coastal upwelling and high productivity (Boersma, 1984b). This species is a major component of the benthic foraminiferal assemblages at Deep Sea Drilling Project (DSDP) Site 532, which was drilled on the southern margin of the Angola Basin at approximately the same depth as Site 1076.

Radiolarians

Radiolarians are present in all of the core-catcher samples from Hole 1076A (Table 5). They are common to abundant in most of the samples, but rare to few in some samples from the lower part of the hole. Good preservation in all investigated samples suggests that the low abundances are probably caused by low productivity and/or dilution by terrigenous sediments, rather than by enhanced dissolution. No apparent reworking has been identified.

The radiolarian fauna indicates a Quaternary age for Site 1076. The absence of *Axoprunum angelinum* indicates that the uppermost cores (175-1076A-1H-CC through 8H-CC) are within either the Pleistocene *Collosphaera tuberosa* Zone or the Pleistocene to Holocene *Buccinosphaera invaginata* Zone of Moore (1995). A finer zonal resolution could not be achieved because of the absence of *B. invaginata.*

The lower part of the section (Cores 175-1076A-9H-CC through 22H-CC) is assigned to the Pleistocene *A. angelinum* Zone or *Amphirhopalum ypsilon* Zone of Moore (1995) based on the presence of *A. angelinum* and the absence of *Lamprocyrtis neoheteroporos*, regardless of the absence of the diagnostic species *Anthocyrtidium angulare* throughout Hole 1076A. The diagnostic species *C. tuberosa*, used to recognize the *A. angelinum* and *A. ypsilon* Zones, is extremely rare. The age-diagnostic species *L. neoheteroporos*, which becomes extinct at 1.07 Ma in tropical oceans, was not found. The oldest sediment could, thus, be younger than 1.07 Ma.

Diatoms

Diatom counts and identification were carried out on smear slides. Opaline phytoliths and silicoflagellates also were counted. Diatoms show marked fluctuations in abundance and preservation (Table 6). In general, diatoms are abundant and well preserved throughout Hole 1076A, except for Samples 175-1076A-3H-CC, 4H-CC, 11H-CC, 14H-CC, 15H-CC, and 16H-CC (Table 6; Fig. 10). Examination of

Table 4. Relative abundance of benthic foraminiferal species and overall abundance of benthic foraminifers at Hole 1076A.

Core, section, interval	Depth (mbsf)	Abundance	*Astrononion novozealandicum*	*Astrononion stelligerum*	*Bolivina ordinaria*	*Bolivina seminuda*	*Bulimina aculeata*	*Bulimina exilis*	*Bulimina marginata*	*Bulimina mexicana*	*Bulimina truncana*	*Cassidulina minuta*	*Cassidulina laevigata*	*Chilostomella oolina*	*Chilostomella ovoidea*	*Cassidulinoides* cf. *bradyi*	*Cibicidoides pachyderma*	*Cibicidoides wuellerstorfi*	*Dentalina* spp.	*Eggerella bradyi*	*Epistominella exigua*	*Epistominella* sp. 1	*Eponides* sp. 1	*Fissurina* spp.	*Fursenkoina* spp.	*Plectofrondicularia* spp.	*Globocassidulina subglobosa*	*Gyroidinoides soldanii*	*Hoeglundina elegans*	*Hyalinea balthica*	*Lenticulina iota*	*Melonis barleeanum*	*Nodosaria* spp.	*Nonionella turgida*	*Oolina* spp.	*Oridorsalis umbonatus*	*Osangularia culter*	*Praeglobobulimina/Globobulimina* group	*Pullenia bulloides*	*Pullenia subcarinata*	*Pyrgo* spp.	*Quadrimorphina allomorphoides*	*Quinqueloculina* spp.	*Sigmoilinopsis schlumbergeri*	*Sphaeroidina bulloides*	*Spiroloculina pusilla*	*Stilostomella* spp.	*Trifarina angulosa*	*Triloculina trigonula*	*Uvigerina auberiana*	*Uvigerina hispidocostata*	*Uvigerina peregrina*	Unidentified	Number of specimens counted
175-1076A-																																																							
1H-CC	4.75	A	5			+	27			14		+	3	+		4	2							2	8				+									5	2		+	4	+			2						2	2	6	7	257
2H-CC	13.21	A					25	2	3	12					+		3					12		1				3					+			1	3	4	+		+	+									15		2	+	295
3H-CC	24.29	A			+	+	1	47	1	+			2		+		+					4				+		1						+		1	+	4	+	+	+	+											+		+	212
4H-CC	33.62	C		+	+	+	3	2	+	2	+		4	+	2	5	+		+					6	+		2	+						+		2	+	7	4		+	6									7	2	5	5	302
5H-CC	43.43	A		+			18	15	+	1	+		+		4	4	2							2	3			+				+	+	+	+	1	+	1	1		2	+									28		2	+	321
6H-CC	52.81	A				+	13	24	+	2	2		+		3	5	+							2	3		+		+						+	2	+	16	2		+	2									13	3	2	2	466
7H-CC	62.46	A			2		34	4		4	7		6	+		+	4	+		+	1			2	+		4	+	3		+	2			2	1	3	+	3		+	+								+	2	2	2	446
8H-CC	71.84	C			+		24	3		3			7			5	19	+					+	3			2		3		+	2			+	2	2	2	2	2									2	1	2	4	274
9H-CC	81.52	C					2	6		2			9		+	2	12	+						4	2		3		5		+	5		+	2	+		4	+	2	+	+	+	2	+							+	2	4	5	366
10H-CC	90.89	C					13	4	4	5	9		10		+	4	17	+	+					4	2		8	+	+					2		+		5					+	2								2	2	8	2	133
11H-CC	100.58	F					14	14		4	+		2		1	4	1	+						1	2		1		+						1	5	14	1		+									3	6	3	6	177
12H-CC	109.89	C					15	12	24	3			2		2	1		+						2	4		+	2	+			+		3		1	5					+									5	4		2	251
13H-CC	119.85	C				2	9	2	+	4	2		18		+	5	5	+			1		4	1	1		3	+	2	3			+		+	1	2		+	+	+	1									3	1	5	301
14H-CC	129.12	F				+	8			4			4		+	+	7	+					6	2	5				13	1	+	3			2	1	2	+	3	2		+			2	1	3	+	2	13	2	3			1	12	2	7	198
15H-CC	138.65	T					P	P		P			P				P	P					P	P					P					P			P					P	P								P			P	23
16H-CC	147.90	T						P					P			P							P	P	P				P					P			P						P									P	P		30
17H-CC	157.86	C					6	7	13	+	1		7			3	4	2					+	6	+	+	4	1	1	+	+		+		1	3		2	3		2									3	6		5	294
18H-CC	166.79	F					35	+	3	9	3					5	8	+						3	2		2		3						+	3		4	2		1										7	1	3	234
19H-CC	176.58	R					2		3	11			19				3							6		2	10								3			5	3		3		2									5	8		11	63
20H-CC	185.98	T						P									P										P							P				P													P	P	P	P	32
21H-CC	195.87	F						33	+	5	4		3		+	3	2							+			4					+			+	1		4	2		2	2									25				3	261
22H-CC	204.93	R					2	2		3								1						9					2							3		2	7		2									45	5	2	3	58

Notes: The relative abundance of benthic foraminiferal species is given as a percentage, where + = <1%. Absolute abundance (per ~20 cm^3 of sediment) of benthic foraminifers is given as A = abundant (>500 specimens); C = common (250–500 specimens); F = few (100–249 specimens); R = rare (50–99 specimens); T = trace (1–49 specimens); and P = present.

Table 5. Stratigraphic distribution of radiolarians at Hole 1076A.

Age	Zone	Core, section, interval	Depth (mbsf)	Abundance	Preservation	*Cycladophora cornutoides*	*Cycladophora davisiana*	*Didymocyrtis tetrathalamus tetrathalamus*	*Eucyrtidium anomalum*	*Lamprocyclas hannai*	*Lamprocyrtis nigriniae*	*Pterocanium praetextum eucolpum*	*Pterocanium trilobum*	*Spongaster tetras tetras*	*Theocorythium trachelium trachelium*	*Phormostichoartus corbula*	*Acanthodesmia viniculata*	*Amphirhopalum ypsilon*	*Collosphaera tuberosa*	*Eucyrtidium calvertense*	*Axoprunum angelinum*
		175-1076A-																			
Quaternary	*B. invaginata–C. tuberosa*	1H-CC	4.75	A	G	P	P	P	P	P	P	P	P	P	P						
Quaternary	*B. invaginata–C. tuberosa*	2H-CC	13.21	C	G	P	P	P		P	P	P	P		P	P					
Quaternary	*B. invaginata–C. tuberosa*	3H-CC	24.29	C	G		P	P		P	P		P		P		P				
Quaternary	*B. invaginata–C. tuberosa*	4H-CC	33.62	A	G			P	P	P	P	P		P			P	P	+		
Quaternary	*B. invaginata–C. tuberosa*	5H-CC	43.43	A	G		P	P	P	P	P	P	P	P	P			P			
Quaternary	*B. invaginata–C. tuberosa*	6H-CC	52.81	A	G	P	P	P	P	P	P	P	P	P			P	P			
Quaternary	*B. invaginata–C. tuberosa*	7H-CC	62.46	A	G	P	P	P	P	P		P	P	P		P	P	P			
Quaternary	*B. invaginata–C. tuberosa*	8H-CC	71.84	A	G	+	P	P		P	P	P	P	P	P	P	P	P		P	
Pleistocene	*A. angelinum–A. ypsilon*	9H-CC	81.51	C	G		P	P	P	P		P	P	P			P				+
Pleistocene	*A. angelinum–A. ypsilon*	10H-CC	90.89	A	G	P	P	P		P	P	P	P	P		P	P				P
Pleistocene	*A. angelinum–A. ypsilon*	11H-CC	100.58	C	G		P	P		P	+	P									P
Pleistocene	*A. angelinum–A. ypsilon*	12H-CC	109.86	A	G		P	P		P	P	P	P	P							P
Pleistocene	*A. angelinum–A. ypsilon*	13H-CC	119.85	F	G		P	P		P	P	P		P			P				P
Pleistocene	*A. angelinum–A. ypsilon*	14H-CC	129.12	F	G			P		P			P	P			P				P
Pleistocene	*A. angelinum–A. ypsilon*	15H-CC	138.65	R	G			P		P				P			P				P
Pleistocene	*A. angelinum–A. ypsilon*	16H-CC	147.9	A	G	P	P	P		P	P	P	P	P		P	P				P
Pleistocene	*A. angelinum–A. ypsilon*	17H-CC	157.86	A	G	P	P	P		P			P	P		P		P			P
Pleistocene	*A. angelinum–A. ypsilon*	18H-CC	166.79	F	G		P	P		P		P	P	P				P			P
Pleistocene	*A. angelinum–A. ypsilon*	19H-CC	176.58	R	G	P		P		P		P	P	P							P
Pleistocene	*A. angelinum–A. ypsilon*	20H-CC	185.98	A	G	P	P	P		P		P	P	P	P	P	P			P	P
Pleistocene	*A. angelinum–A. ypsilon*	21H-CC	195.87	C	G		P	P		P			P	P		P				P	P
Pleistocene	*A. angelinum–A. ypsilon*	22H-CC	204.93	A	G		P	P	P	P			P	+			P			P	P

Notes: Occurrence is indicated by P = present and + = one specimen per slide. Abundance: A = abundant; C = common; F = few; and R = rare. Preservation: G = good. *B. invaginata* = *Buccinosphaera invaginata; C. tuberosa* = *Collosphaera tuberosa; A. angelinum* = *Axoprunum angelinum; A. ypsilon* = *Amphirhopalum ypsilon.*

Table 6. Overall diatom abundance and relative contribution of the dominant species or assemblages at Hole 1076A.

Core, section, interval	Depth (mbsf)	Overall abundance	Overall preservation	*Thalassionema nitzschioides* (%)	*Chaetoceros* resting spores (%)	*Skeletonema costatum*	*Thalassiosira* spp.	Freshwater assemblage (%)	Phytoliths	Silicoflagellates
175-1076A-										
1H-CC	4.75	A-C	2.0	33.3	25.8	T	T	34.8		T
2H-CC	13.21	A	2.0	19.1	47.8	T	R	16.5		T
3H-CC	24.29	T	1.0				T		T	
4H-CC	33.62	T	1.0	F	R			R		
5H-CC	43.43	A	2.0	56.4	14.9	T	T	18.8		T
6H-CC	52.81	C	2.5	37.9	29.5	21.1	T	5.2		
7H-CC	62.46	A	2.5	52.5	32.5	T	T	3.8	T	
8H-CC	71.84	C	2.0	29.8	54.6	T	T	9.2		T
9H-CC	81.52	A	2.0	53.9	20.9		T	10.4		
10H-CC	90.89	A	2.0	36.7	33.3	11.9	R	8.1		T
11H-CC	100.58	T	1.0	T					T	
12H-CC	109.89	A	2.0	40.1	50.1	T	R	3.2	T	T
13H-CC	119.85	F-C	2.0	54.4	33.3		T	5.5	T	
14H-CC	129.12	T	1.0	T						
15H-CC	138.65	T	1.0	T	T			T		
16H-CC	147.90	R	1.0	F	T				T	
17H-CC	157.86	A	1.5	38.3	45.8	T	T	9.3	T	T
18H-CC	166.79	A	2.0	53.8	38.8		R	0.2		T
19H-CC	176.58	A	2.0	56.3	31.7	T	R	6.7	T	T
20H-CC	185.98	C	1.5	32.6	31.9	T	25.3	4.5		R
21H-CC	195.87	C	1.0	61.4	27.9		R	1.4	T	T
22H-CC	204.93	C	1.0	45.1	37.0	T	6.4	3.3		

Notes: Includes diatom upwelling and freshwater assemblages, opaline phytoliths, and silicoflagellates (in percentages). Abundance: A = abundant; T = trace; C = common; F = few; and R = rare. Preservation: G = good; M = moderate; and P = poor.

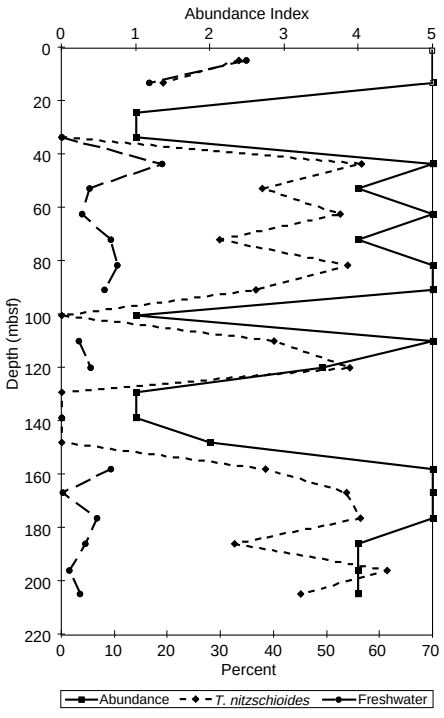

Figure 10. Diatom abundance (z-axis), and percent *T. nitzschioides* and freshwater diatoms (x-axis) at Hole 1076A. Abundance index: 5 = abundant, 4 = common, 3 = few, 2 = rare, 1 = trace, and 0 = barren. *T. nitzschioides* is an upwelling indicator in the Congo Fan area.

the core-catcher samples from Hole 1076A indicates a Pleistocene age for this hole. Samples 175-1076A-1H-CC through 10H-CC are assigned to the *Pseudoeunotia doliolus* Zone. Diatom biostratigraphic marker species are lacking downhole. However, the silicoflagellate *Mesocena quadrangula* is present in Samples 175-1076A-17H-CC (LO at 0.8 Ma) through 20H-CC (first common occurrence at 1.0 Ma; Locker, 1996) and may be used as a biostratigraphic marker instead.

The diatom flora is dominated by upwelling-indicator species (>60% of total diatom assemblage *Thalassionema nitzschioides* var. *nitzschioides* and *Chaetoceros* resting spores and setae; see Table 6), accompanied by freshwater taxa (e.g., *Aulacoseira granulata, A. islandica,* and *Cyclotella* spp.), and neritic species (e.g., *Actinoptychus senarius*). Two distinct pulses of the coastal species *Skeletonma costatum* are observed in Samples 175-1076A-6H-CC (~21%) and 10H-CC (~12%), respectively. Species characteristic of open-ocean conditions (e.g., *Alveus* [= *Nitzschia*] *marinus, Azpeitia* spp., and *Rhizosolenia robusta*) were less abundant than here than at Hole 1075A. In general, diatom assemblages characterize Hole 1076A as a coastal upwelling site with variable freshwater input (Fig. 7; also see "Site 1075" chapter, this volume).

As at Hole 1075A, the presence of freshwater diatoms at Hole 1076A is attributed to supply by the Congo River, and high abundances may be interpreted as signals for humid intervals on the African continent (e.g., Jansen et al., 1989). The average contribution of the freshwater assemblage is somewhat higher than at Hole 1075A (6.4% vs. 3.5%). Peaks are seen in the upper 40 m (>15%) and in Samples 175-1076A-8H-CC through 10H-CC (8%–10%) and 175-1076A-17H-CC. Opaline phytoliths are present only sporadically and in low numbers (Table 6); therefore, the ratio PhFD (phytoliths/[freshwater diatoms + phytoliths] × 100) is not given.

Table 7. Tensor tool–orientation data for cores from Holes 1076A, 1076B, 1076C, and 1076D.

Core, section	MTF (°)	Inclination angle
175-1076A-		
3H	206	2.38
4H	124	2.33
5H	16	2.11
6H	29	2.14
7H	231	2.12
8H	231	2.15
9H	277	1.86
10H	191	1.88
11H	26	1.87
12H	357	1.78
13H	39	1.85
14H	69	1.76
15H	81	1.84
16H	98	1.83
175-1076B-		
4H	68	0.72
5H	295	1.14
6H	297	2.00
7H	293	1.62
175-1076C-		
18H	222	0.67
19H	74	0.68
20H	173	0.71
21H	187	0.69
22H	247	0.52
175-1076D-		
3H	273	1.20
4H	237	1.49
5H	173	1.53

Notes: The orientation parameter (MTF) is the angle in degrees between magnetic north and the double line marked on the center of the working half of the core. The local declination anomaly is 6°W.

PALEOMAGNETISM

The investigation of magnetic properties at Site 1076 included the measurement of bulk susceptibility of whole-core sections and the natural remanent magnetization (NRM) of archive-half sections. The Tensor tool was used to orient Hole 1076A for Cores 3H through 16H, Hole 1076B for Cores 4H through 7H, Hole 1076C for Cores 18H through 22H, and Hole 1076D for Cores 3H through 5H (Table 7). The remaining cores from each hole were not oriented because of technical problems with the Tensor tool.

Natural Remanent Magnetization and Magnetic Susceptibility

Measurements of NRM were made on all archive-half core sections from Holes 1076A, 1076C, and 1076D. Cores 175-1076B-1H through 3H were measured, but the remaining cores from Hole 1076B were not measured because of pronounced sediment disturbance. Sections from Hole 1076A were demagnetized by alternating field (AF) at 10 and 20 mT, and sections from Holes 1076B, 1076C, and 1076D were demagnetized by AF at 20 mT only.

Magnetic susceptibility measurements were made on whole cores from all four holes as part of the MST analysis (see "Physical Properties" section, this chapter), except for Cores 175-1076B-4H through 7H, which were not measured because of technical difficulties with the MST. Magnetic susceptibility was relatively low, on the order of 10^{-5} (SI volume units; Fig. 11).

The intensity of NRM after 20-mT demagnetization from the three measured holes is similar in magnitude, ranging from ~10^{-5} to ~10^{-3} A/m (Fig. 12, left panel). Within the upper 50 mbsf of Holes 1076A and 1076C, the intensity is on the order of 10^{-3} to 10^{-4} A/m. The NRM decreases gradually (from ~10^{-4} to ~10^{-5} A/m) between 40 and 90 mbsf, below which it increases rapidly to 10^{-3} A/m and once again decreases gradually with depth. A similar trend was observed in the magnetic susceptibility, which increases rapidly below ~95 mbsf (Fig. 11).

A relatively stable magnetic component was preserved in sediments from all three holes, which allowed the determination of the magnetic polarity. A magnetic overprint with steep positive inclinations, which was probably acquired during drilling, was usually erased by 20-mT demagnetization. Directions of the NRM below ~140 mbsf, however, show relatively large scatter. This suggests that secondary magnetizations still remain and are probably a viscous remanent magnetization and/or chemical remanent magnetization caused by diagenetic growth or dissolution of magnetic minerals.

Magnetostratigraphy

We identified the polarity of the NRM from the declinations and inclinations. Data from the Tensor orientation tool were available for most of Hole 1076A, which facilitated interpretation of reversals in terms of the geomagnetic time scale. Changes of inclination with polarity transitions were difficult to interpret because of the low latitude of this site (an inclination of –10° is expected from the geocentric axial dipole model) and the magnetic overprint (Fig. 12, right panel).

The Brunhes/Matuyama polarity transition (0.78 Ma; Berggren et al., 1995) occurs between 132 and 138 mbsf at Hole 1076A and between 136 and 140 mbsf at Hole 1076C; the Brunhes/Matuyama boundary was not identified at Hole 1076D (Fig. 12, middle panel). The thickness of sediments, which records a polarity transition, should be ~1.5 m at these holes, assuming that the sedimentation rate is ~150 m/m.y. and a polarity transition completes within 10 k.y. However, the large scatter of the remanent directions and the incomplete Tensor data made it difficult to determine the exact position of the boundary. The termination and beginning of the Jaramillo Subchron (C1r.1n), the ages of which are 0.99 and 1.07 Ma (Berggren et

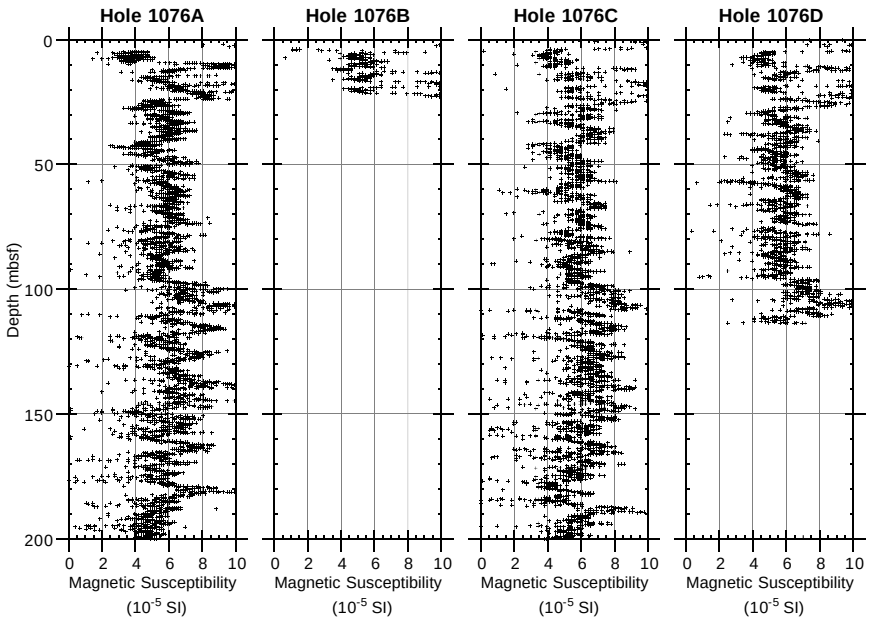

Figure 11. Magnetic susceptibilities from MST data (volume corrected) for Holes 1076A, 1076B, 1076C, and 1076D.

al., 1995), respectively, occur at ~156–158 and 167–170 mbsf at Hole 1076A and at about 165–167 and 175–178 mbsf at Hole 1076C.

We observed a possible short reversal event in the Brunhes Chron. It occurs at all four holes: 16–22 mbsf at Hole 1076A (the bottom is not clear because of a gap); 20 mbsf to the bottom of Hole 1076B (23 mbsf); 20–26 mbsf at Hole 1076C; and 20–25 mbsf at Hole 1076D. Figure 13 displays this record from Cores 175-1076D-2H through 4H. All holes except Hole 1076C show declinations of almost 180° opposite the average Brunhes declination. This is possibly the Blake event, considering the calcareous nannofossil age of 90 ka at 16 mbsf at Hole 1076A (see "Biostratigraphy and Sedimentation Rates" section, this chapter). The Blake event is considered to have occurred during the earlier part of the $\delta^{18}O$ Stage 5, at ~120 ka (Tric et al., 1991; Tucholka et al., 1987). The duration of the Blake event is not well constrained, but it is probably 10 k.y. or less. The occurrence of the event through several meters in the sediments suggests an extremely high sedimentation rate (~500 m/m.y.) during Stage 5 at this site.

Another rapid change in declinations was observed in Core 175-1076A-8H (74 mbsf). It is, however, uncertain whether this is of geomagnetic field origin or whether it reflects a coring disturbance. Other anomalous directions, shown in Figure 12, occur at core boundaries and are thus considered to be caused by sediment disturbance.

COMPOSITE SECTION

MST physical properties data on magnetic susceptibility, GRAPE, and *P*-wave velocity were measured at 2- to 4-cm intervals, and discrete measurements of spectral reflectance were made at 2- to 4-cm intervals for Holes 1076A, 1076C, and 1076D. Quantitative and graphic correlation of features present in the physical parameter measurements of adjacent holes were used to establish depth continuity of the stratigraphic sequence. This process was used to determine intercore depth offsets of adjacent holes and to establish a composite depth scale (in mcd) for Site 1076 (Table 8). The stratigraphic sequence was demonstrated to be continuous to 129 mbsf. Cores from Holes 1076A and 1076D, drilled between 129 and 204 mbsf, were largely at equal depths, obfuscating the determination of depth continuity below 129 mbsf.

High gas content in the sediments caused expansion, disturbance, and numerous voids in the recovered cores. These voids generate considerable noise in the MST measurements, particularly in the GRAPE density and magnetic susceptibility data, where the volume reduction caused by voids and cracks reduces the amplitude. *P*-wave measurements were too noisy to be useful in determining composite depths. Extensive filtering of the measured parameters (GRAPE, magnetic susceptibility, and spectral reflectance) was necessary before constructing a composite section. Filtering procedures are the same as those used at Site 1075 (see "Composite Section" section, "Site 1075" chapter, this volume).

Magnetic susceptibility and color reflectance (red/blue ratio [650 nm/450 nm]) were the primary records used for establishing the depth composite record (Fig. 14). GRAPE density and color reflectance (chromaticity b*) parameters were also used for control and refinement.

Relative correlation of the sedimentary sections was very good; however, stretching and core compression are observed on length scales <9.5 m and lead to locally observed intercore disagreements. Additional processing is required to correct for these distortions. Below 137 mcd, some relative core-to-core adjustments could be made with adjacent Holes 1076A and 1076C. Following construction of the composite depth section for Site 1076, a single spliced record was assembled from the aligned cores (Fig. 15). The Site 1076 spliced record can be used as a sampling guide to recover a single sedimentary sequence. Tie points for these splices are given in Table 9. Correlations below 140 mcd are tentative. Growth of the mcd composite depths relative to the mbsf drilled was ~11% (Fig. 16).

INORGANIC GEOCHEMISTRY

Sixteen interstitial water samples were collected from Hole 1076A and analyzed (Table 10). The sampling protocol called for gathering one 10-cm-long whole-round interval from each core from the surface to ~100 mbsf and one 10-cm-long whole-round interval from approximately every third core thereafter. The shallowest sample was taken from 1.4 mbsf and the deepest from 202.2 mbsf, ensuring coverage of diagenetic processes throughout the complete section cored. Headspace samples (see "Organic Geochemistry" section, this

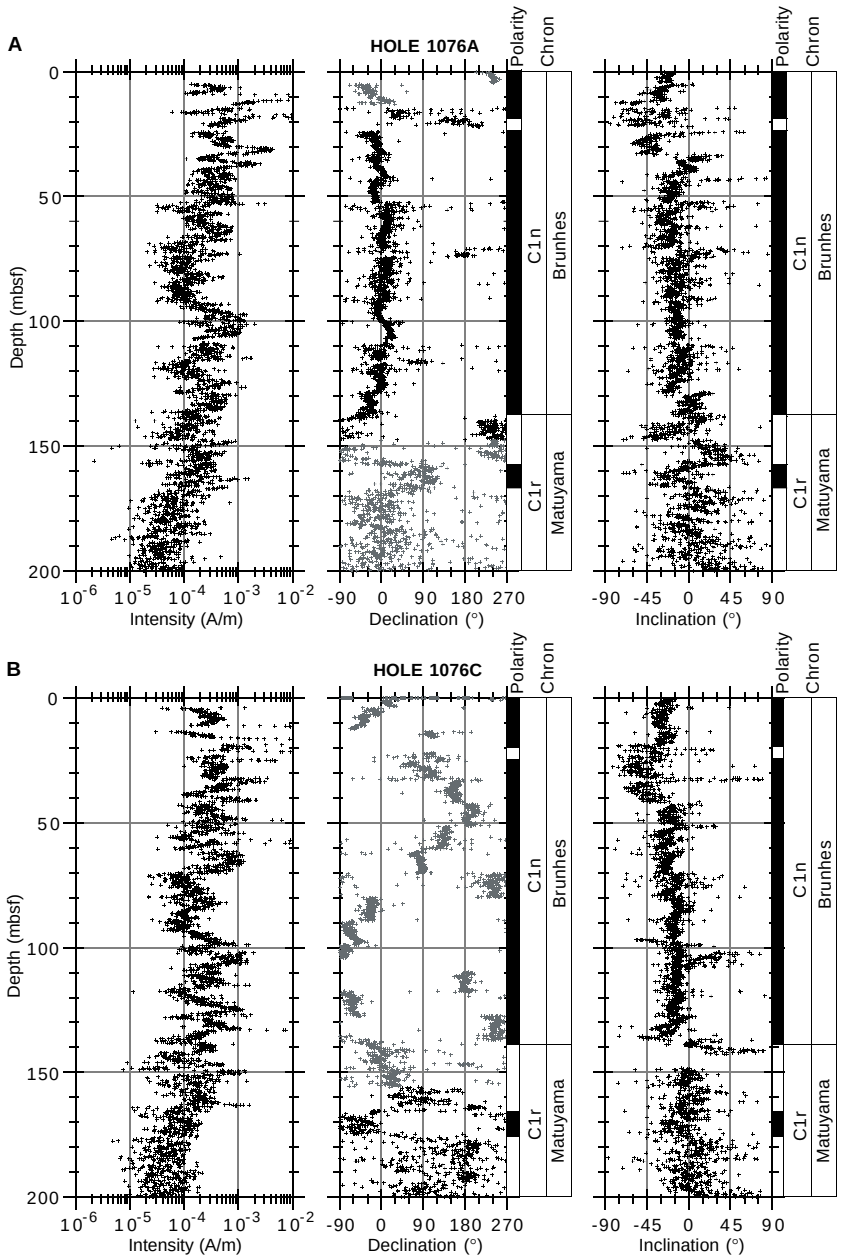

Figure 12. NRM intensity, declination, inclination, and magnetostratigraphic interpretation after 20-mT demagnetization. Black symbols = Tensor corrected; gray symbols = uncorrected. Polarity shading: black = normal and white = reversed. **A.** Hole 1076A. **B.** Hole 1076C. (Continued on next page.)

chapter) were taken immediately adjacent to each interstitial water whole-round sample, thereby providing a comparable high-resolution data set for volatile hydrocarbons.

Alkalinity, Sulfate, and Ammonium

Downcore profiles of alkalinity, sulfate, and ammonium (Fig. 17) reflect the degradation of organic matter. The high total organic carbon concentrations at this site (see "Organic Geochemistry" section, this chapter) are responsible for the very steep decline in dissolved sulfate as well as the sharp increase in alkalinity below the seafloor. Concomitant with the sulfate decrease and alkalinity increase, ammonium also increases rapidly through the uppermost 5–10 mbsf but continues to increase to the bottom of the hole, recording both shallow and deep degradation of organic matter. Below the initially rapid increase in alkalinity, there is a gradual increase to a broad maximum of ~35 mM from 30–70 mbsf, a pronounced minimum centered near 150 mbsf, and a clear increase in the deepest section of the sedimentary succession. The deep alkalinity increase will be discussed below in the context of the distributions of dissolved Ca^{2+}, Mg^{2+}, and Sr^{2+}.

The depletion of dissolved sulfate within the uppermost 20 mbsf (Fig. 17) occurs at a shallower depth than was observed at Site 1075, reflecting the higher sedimentation rate at Site 1076. The effect of higher sedimentation rate is to hasten the isolation of the sedimented organic matter from overlying oxygenated seawater and, thus, to promote anaerobic degradation.

Calcium, Magnesium, and Strontium

As at Site 1075, organic degradation also drives carbonate dissolution and precipitation, recorded in the distributions of dissolved Ca^{2+}, Mg^{2+}, and Sr^{2+} (Fig. 18). The strong decreases in Ca^{2+} and Mg^{2+} initially occur at depths shallower than at Site 1075. Likely phases responsible for the decreases in dissolved Ca^{2+} and Mg^{2+} include

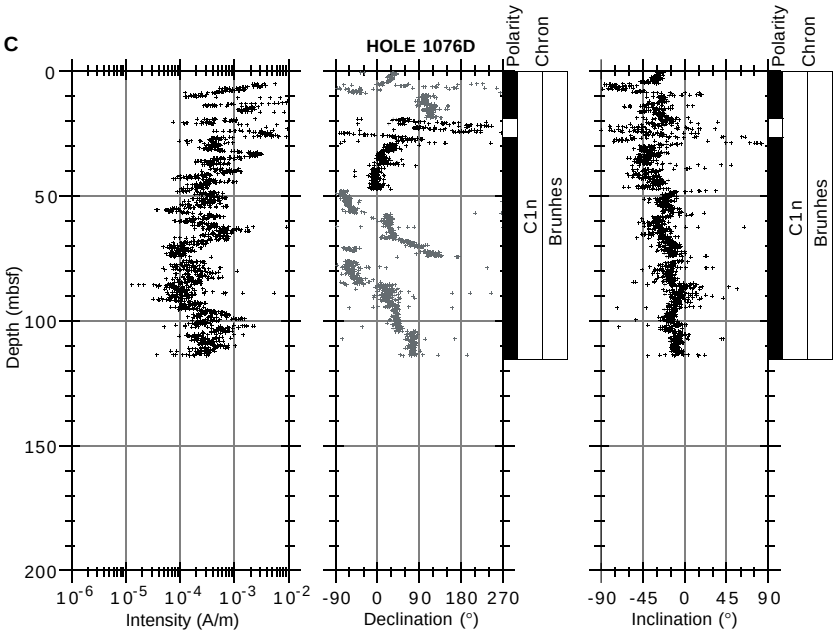

Figure 12 (continued). **C**. 1076D.

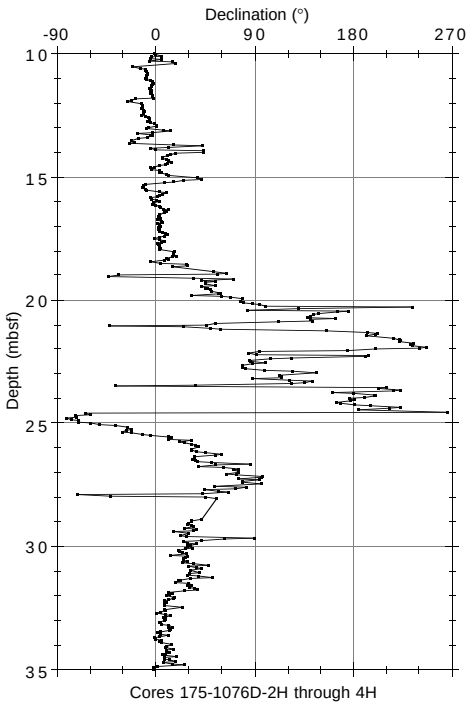

Figure 13. Possible Blake event from Cores 175-1076D-2H through 4H (20–25 mbsf).

authigenic carbonates (e.g., dolomite), clays, and authigenic apatite. Keeping in mind that the uppermost three data points in the dissolved Sr^{2+} profile are within analytical precision, the dissolved Sr^{2+} increases over the uppermost 50 mbsf reflect diagenetic dissolution of biogenic calcite.

As we propose for Site 1075, there may be more than one distinct sink of dissolved Mg^{2+} at Site 1076. Extrapolating the deeper trend of Mg^{2+} depletion, presumably caused by authigenic clay mineral formation (at depths >50 mbsf), to stratigraphically shallower levels up to the bottom-water value of 53 mM (Fig. 18), we infer that the additional Mg^{2+} drawdown (see uppermost shaded region in Fig.18) is caused by dolomite formation. Stoichiometrically, the precipitation of dolomite should cause equal consumption of dissolved Ca^{2+} and Mg^{2+}. The preliminary observations here suggest that the excess decrease of Mg^{2+} approximately balances the decrease in dissolved Ca^{2+} (note the different horizontal axis scales in Fig. 18). Postcruise mass balance calculations of the Ca^{2+}, Mg^{2+}, and Sr^{2+} budgets will provide further information about these hypothesized authigenic processes.

The increases in alkalinity (Fig. 17), dissolved Ca^{2+}, and dissolved Sr^{2+} that occur below 130–150 mbsf suggest additional dissolution of biogenic calcite at this greater depth. Because there also appears to be a region of increased Mg^{2+} uptake through this depth range (see deeper shaded region in Fig. 18), dolomitization may also be occurring. This hypothesis is consistent with the observation that the Mg^{2+} gradient at Site 1076 (a decrease of 27 mM/200 m) is stronger than that at Site 1075 (19 mM/200 m) where we considered only authigenic clay mineral formation as a sink for Mg^{2+}.

Silica and Phosphate

Dissolved silica concentrations increase very rapidly through the uppermost 5 m of sediment (Fig. 19), recording the dissolution of biogenic opal. Concentrations continue to gradually increase downcore. The maximum in dissolved silica at ~150 mbsf corresponds to an interval in which diatoms are rare or absent (see "Biostratigraphy and Sedimentation Rates" section, this chapter).

Dissolved phosphate increases very rapidly to a maximum value of ~110 µM within the uppermost 20 mbsf. The rate of increase is far greater than that observed at Site 1075; this is consistent with the sharper increase in alkalinity at Site 1076 and the sharp decrease in dissolved sulfate, as described above, all of which reflect intense degradation of organic matter in the shallowest buried sediments. The decrease in dissolved phosphate with depth reflects the presence of a phosphate sink, which is most likely the formation of authigenic apatite.

Sodium and Potassium

Concentrations of both dissolved Na^{+} and K^{+} increase with depth downcore (Fig. 20). The behavior of these components most likely reflects reactions with clay minerals throughout the sequence.

Table 8. Offsets applied to cores from Holes 1076A, 1076C, and 1076D.

Core	Depth (mbsf)	Offset (m)	Composite depth (mcd)
175-1076A-			
1H	0.0	0.00	0.00
2H	4.8	2.86	5.72
3H	14.3	5.93	9.00
4H	23.8	4.46	2.99
5H	33.3	6.22	7.98
6H	42.8	5.52	4.82
7H	52.3	6.61	7.70
8H	61.8	7.81	9.01
9H	71.3	8.74	9.67
10H	80.8	9.44	10.14
11H	90.3	10.26	11.08
12H	99.8	11.40	12.54
13H	109.3	12.26	13.12
14H	118.8	11.84	11.42
15H	128.3	11.48	11.12
16H	137.8	11.48	11.48
17H	147.3	11.48	11.48
18H	156.8	11.48	11.48
19H	166.3	12.12	12.76
20H	175.8	12.12	12.12
21H	185.3	12.12	12.12
22H	194.8	12.12	12.12
175-1076C-			
1H	0.0	0.24	0.24
2H	3.6	0.98	1.72
3H	13.1	1.64	2.30
4H	22.6	2.56	3.48
5H	32.1	2.70	2.84
6H	41.6	4.00	5.30
7H	51.1	5.46	6.92
8H	60.6	6.29	7.12
9H	70.1	7.66	9.03
10H	79.6	9.30	10.94
11H	89.1	9.46	9.62
12H	98.6	11.3	13.14
13H	108.1	11.88	12.46
14H	117.6	11.74	11.60
15H	127.1	11.74	11.74
16H	136.6	12.34	12.94
17H	146.1	12.34	12.34
18H	155.6	11.98	11.62
19H	165.1	11.98	11.98
20H	174.6	11.98	11.98
21H	184.1	11.98	11.98
22H	193.6	11.98	11.98
175-1076D-			
1H	0.0	0.12	0.12
2H	9.0	1.66	3.20
3H	18.5	1.72	1.78
4H	28.0	2.66	3.60
5H	37.5	3.60	4.54
6H	47.0	5.98	8.36
7H	56.5	5.43	4.88
8H	66.0	8.36	11.29
9H	75.5	9.20	10.04
10H	85.0	10.70	12.20
11H	94.5	10.74	10.78
12H	104.0	12.16	13.58

Note: The offsets transform ODP standard depth values in meters below seafloor (mbsf) to meters composite depth (mcd).

Salinity and Chloride

The initial downcore decrease of salinity through the upper 30 mbsf (Fig. 21) appears to be caused by the decrease in dissolved sulfate, Ca^{2+}, and Mg^{2+} through this interval. The increase below 150 mbsf reflects the increase in many of the dissolved constituents through these deeper sections. The concentration of dissolved Cl^- increases relatively smoothly downcore. The cause of this increase remains unclear at this time, but the gradual increase at Site 1076 is different from the sharp increase at Site 1075 (for which we call on a diffusional glacial signal).

Neither the salinity nor the dissolved Cl^- profile suggests the presence of gas hydrate at any interval within the uppermost 200 mbsf. There is no chemical evidence of dilution by H_2O that would have been released by hydrate dissolution during recovery.

ORGANIC GEOCHEMISTRY

Calcium carbonate and organic carbon concentrations were measured on sediment samples from Hole 1076A (Table 11). Organic matter atomic carbon/nitrogen (C/N) ratios and Rock-Eval pyrolysis analyses were employed to determine the type of organic matter contained within the sediments. High headspace gas contents were measured, and routine monitoring of the sedimentary gases was done for drilling safety.

Inorganic and Organic Carbon Concentrations

Concentrations of carbonate carbon are low in Site 1076 sediments. They vary between 1.9 and 0.1 wt% (Table 11). The maximum carbonate carbon concentration is equivalent to 16 wt% sedimentary $CaCO_3$, and most sediment samples contain <5 wt% $CaCO_3$. These generally low concentrations agree with the paucity of coccoliths and the high abundances of opaline and continental clastic material at this site (see "Biostratigraphy and Sedimentation Rates" section, this chapter). The range in concentrations reflects a varying combination of changes in biological production of calcareous material, dilution by noncalcareous components, and carbonate dissolution fueled by oxidation of organic matter.

TOC determinations were done on a smaller number of Hole 1076A sediment samples than carbonate determinations because of the generally uniform lithology. TOC values range from 4.32 to 0.93 wt% (Table 11) and average 2.56 wt%. The concentrations are ~10 times greater than the average of 0.3 wt% given by McIver (1975) based on DSDP Legs 1–33, a value that can be considered representative of typical deep-sea sediments. The high TOC concentrations at this site may be ascribed to a combination of high supply from elevated paleoproductivities and a high rate of accumulation enhancing preservation of the organic matter.

Organic Matter Source Characterization

Organic C/N ratios were calculated for Site 1076 samples using TOC and total nitrogen concentrations to help identify the origin of their organic matter. Site 1076 C/N ratios vary from 17.2 to 4.5 (Table 11). The C/N ratios average 13.9, a value that is intermediate between unaltered algal organic matter (5–8) and fresh land-plant material (25–35; e.g., Emerson and Hedges, 1988; Meyers, 1994). It is likely that these organic carbon–rich sediments contain a mixture of partially degraded algal material and detrital continental organic matter. Preferential loss of nitrogen-rich, proteinaceous matter can elevate the C/N ratios of algal organic matter during settling to the seafloor (Meyers, 1997).

A Van Krevelen–type plot of the hydrogen index (HI) and oxygen index (OI) values indicates that the sediments contain a mixture of type II (algal) and type III (land-derived) organic matter (Fig. 22). This source assignment for the organic matter is consistent with the intermediate C/N ratios for these samples, which also suggests that the organic matter is a mixture of marine and continental material. An equally likely possibility, however, is that the sediments principally contain algal-derived organic matter that has been altered by microbial processing during early diagenesis. Well-preserved type II organic matter has high HI values (Peters, 1986), which can be lowered by microbial oxidation (Meyers, 1997). The low HI values of fresh type III organic matter, however, cannot become elevated by postdepositional alteration. In general, Hole 1076A sediments having

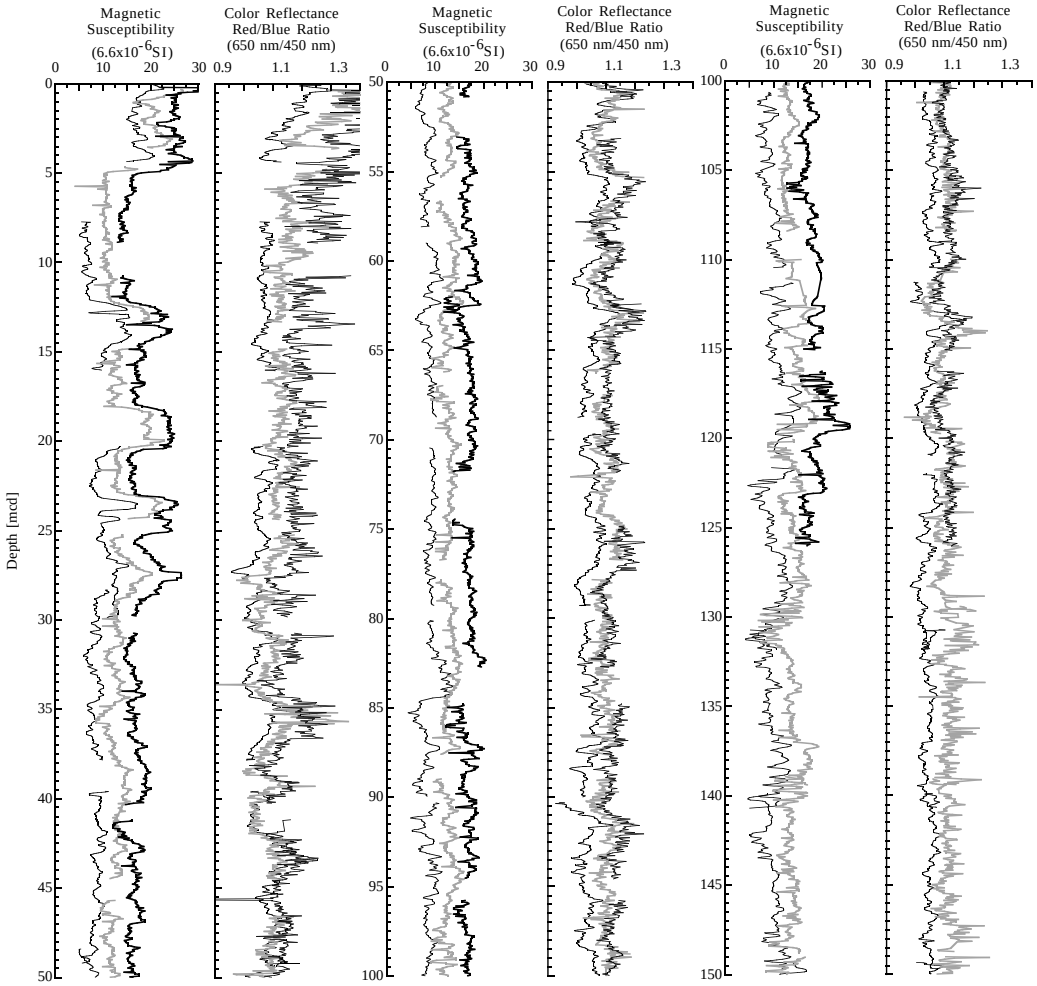

Figure 14. Composite section for Site 1076. Magnetic susceptibility and color reflectance (red/blue ratio [650 nm/450 nm]) are plotted for Holes 1076A (thin black line), 1076C (gray line), and 1076D (thick black line). Downhole logs are shown in meters composite depth (mcd). Offsets have been applied for clarity.

higher Rock-Eval TOC values also have higher HI values (Table 12). This relationship is consistent with partial oxidation of algal organic matter. Further evidence of substantial amounts of in situ organic matter degradation exists in the large increases in alkalinity and decreases in sulfate in the interstitial waters of Site 1076 sediments (see "Inorganic Chemistry" section, this chapter).

Variable T_{max} values (Table 12) reflect poorly defined S_2 peaks and not actual thermal maturities of organic matter. Those samples in which the geometry of S_2 peaks was sharp have relatively low T_{max} values, showing that organic matter is thermally immature with respect to petroleum generation (Peters, 1986) and therefore contains little detrital organic matter derived from erosion of ancient sediments and transported to this site by the Congo River.

Headspace Gases

Sediments from Hole 1075A had high gas content. Gas pressures became great enough in sediments below Core 175-1076A-15H (138 mbsf) to require perforating the core liner to relieve the pressure and alleviate core expansion. Natural gas analyses determined that much of this gas was CO_2 (Table 13). Hydrogen sulfide could be detected by nose, but not by hydrogen sulfide–sensing instruments having a sensitivity of ~1 ppm, in Cores 175-1076A-3H through 5H (18–39 mbsf).

Methane (C_1) first appears in headspace gas samples in Hole 1076A sediments at 28.3 mbsf. Concentrations rapidly increase and become significant in sediments below 35 mbsf (Fig. 23). As at Site 1075, high methane/ethane (C_1/C_2) ratios and the absence of major contributions of higher molecular weight hydrocarbon gases (Table 13) indicate that the methane is biogenic, as opposed to thermogenic, in origin. A biogenic origin of the methane is supported by the disappearance of interstitial sulfate at approximately the same sub-bottom depth where methane concentrations begin to rise (see "Inorganic Geochemistry" section, this chapter). As noted by Claypool and Kvenvolden (1983), the presence of interstitial sulfate inhibits methanogenesis in marine sediments.

PHYSICAL PROPERTIES

Shipboard measurements at Site 1076 included nondestructive, near-continuous measurements of GRAPE density, compressional (*P*-wave) ultrasonic velocity, and magnetic susceptibility on whole-round sections of all cores from each hole using the MST (see

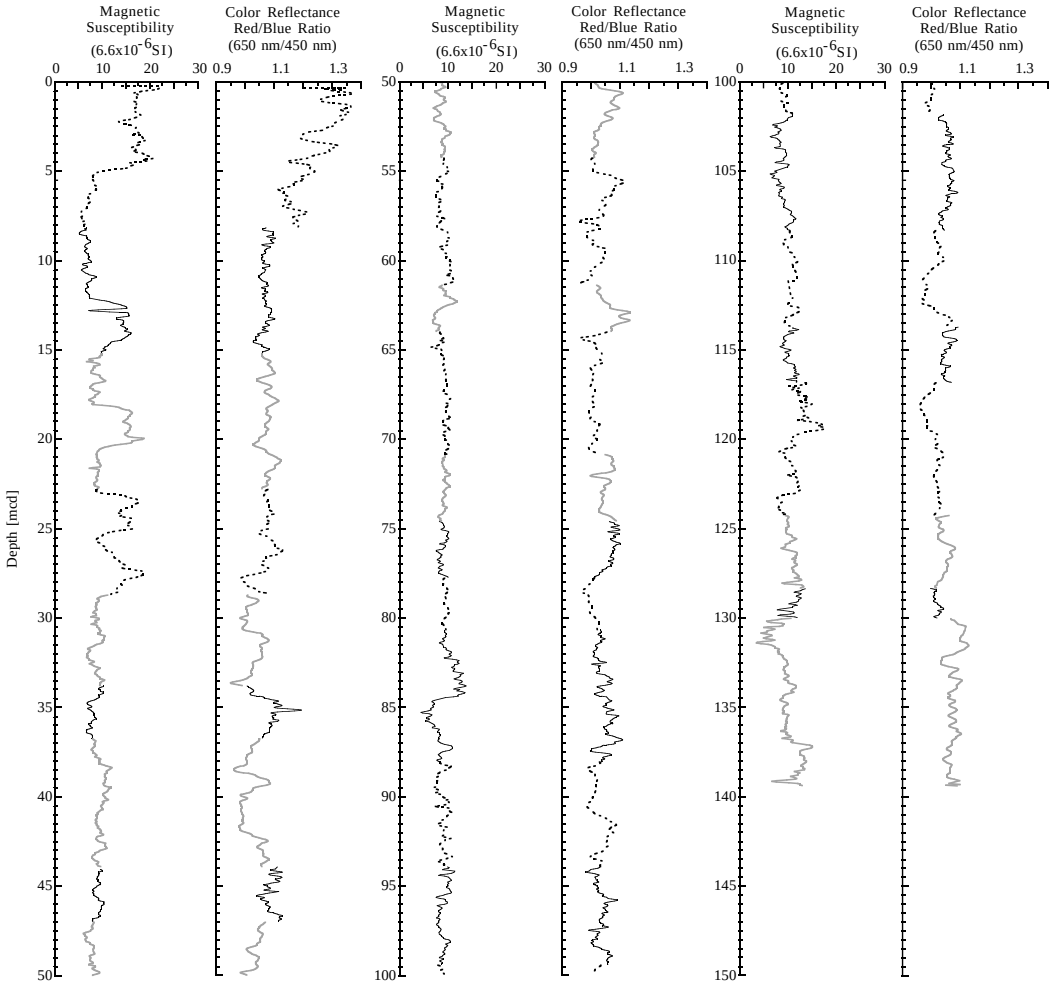

Figure 15. Spliced records for magnetic susceptibility and color reflectance (red/blue ratio [650 nm/450 nm]) plotted in meters composite depth (mcd). Cores from three holes at Site 1076 have been used for the spliced record: solid black line = Hole 1076A, gray line = Hole 1076C, and dashed line = Hole 1076D.

"Explanatory Notes" chapter, this volume). Many core sections were disturbed because of degassing processes within the sediments (see "Lithostratigraphy" section, this chapter).

Index properties (gravimetric density) measurements were conducted on one or two samples (volume = ~10 cm^3) per section on all cores (see "Explanatory Notes" chapter, this volume). Method C was utilized at this site.

Ultrasonic compressional (*P*-wave) velocities were determined at a resolution of two per section, and undrained vane-shear measurements at a resolution of one per section. The ultrasonic transducers of the digital sediment velocimeter could be inserted into the soft sediments down to a depth of ~35 mbsf. Below that depth, the signal quality degraded considerably, probably because of higher gas content in pores. Therefore, the modified Hamilton Frame had to be used farther downcore.

Multisensor Track

The sampling rate for ultrasonic compressional wave velocity, magnetic susceptibility, and GRAPE density was 2 cm for the upper 60 m and was changed to 4 cm after Core 175-1076A-6H (Figs. 24–26). MST data are included on CD-ROM (back pocket, this volume). During the data analysis of the MST velocity data, it became evident that the acquisition system did not work properly. Analysis revealed a large and random scatter (Fig. 24A) caused by the limited core quality in combination with technical problems. A comparison between MST data (solid line) and discrete velocity values (solid circles) is shown in Figure 24A and in more detail in Figures 24B and C. The near-continuous MST *P*-wave values shown in Figures 24B and C were filtered and smoothed to fit into the most likely range of values, based on the discrete velocity values. It must be stated that the MST velocity logs measured at this site must be treated with great caution and require thorough editing.

GRAPE density and magnetic susceptibility logs show a higher quality and a pronounced cyclicity. After thorough editing, these data will be suitable to carry out detailed time-series analyses and to reconstruct even fast changes in environmental conditions.

Velocities

The near-continuous velocity profile recorded with the MST shows a very high level of noise and scatter, as described above. The disturbance of the sediments along most of the core sections precluded good coupling between the transducer elements and the sediment in the core liners and reduced the signal strength, inhibiting good determinations of first arrival times. Figures 24A and B display raw MST data (dots) and a filtered velocity log (solid line) compared with discrete velocity values (solid circles).

Between 0 and ~35 mbsf, discrete velocities tend to increase slightly from 1470 to 1535 m/s because of compaction and display

Table 9. List of splice tie points used to create the continuous "spliced" stratigraphic sequence for Site 1076.

Hole, core, section, interval (cm)	Depth (mbsf)	Composite depth (mcd)	Whether tied	Hole, core, section, interval (cm)	Depth (mbsf)	Composite depth (mcd)
1076D-1H-6, 52	8.02	8.14	Tie to	1076A-2H-1, 48	5.28	8.14
1076A-2H-6, 4	12.34	15.20	Tie to	1076C-3H-1, 45	13.56	15.20
1076C-3H-6, 52	21.12	22.76	Tie to	1076D-3H-2, 104	21.04	22.76
1076D-3H-6, 96	26.96	28.68	Tie to	1076C-4H-3, 52	26.12	28.68
1076C-4H-6, 112	31.22	33.78	Tie to	1076A-4H-4, 102	29.32	33.78
1076A-4H-6, 96	32.26	36.72	Tie to	1076C-5H-2, 40	34.02	36.72
1076C-5H-7, 8	41.20	43.90	Tie to	1076A-5H-3, 138	37.68	43.90
1076A-5H-5, 146	40.76	46.98	Tie to	1076C-6H-1, 137	42.98	46.98
1076C-6H-6, 112	50.22	54.22	Tie to	1076D-6H-1, 124	48.24	54.22
1076D-6H-6, 88	55.38	61.36	Tie to	1076C-7H-4, 29	55.90	61.36
1076C-7H-5, 140	58.50	63.96	Tie to	1076D-7H-2, 52	58.53	63.96
1076D-7H-6, 140	65.40	70.83	Tie to	1076C-8H-3, 93	64.54	70.83
1076C-8H-6, 16	68.26	74.55	Tie to	1076A-8H-4, 44	66.74	74.55
1076A-8H-6, 56	69.91	77.72	Tie to	1076D-8H-3, 36	69.36	77.72
1076D-8H-5, 28	72.28	80.64	Tie to	1076A-9H-1, 60	71.90	80.64
1076A-9H-6, 68	79.30	88.04	Tie to	1076D-9H-3, 33	78.84	88.04
1076D-9H-7, 20	84.70	93.90	Tie to	1076A-10H-3, 65	84.46	93.90
1076A-10H-7, 24	89.94	99.38	Tie to	1076D-10H-3, 68	88.68	99.38
1076D-10H-5, 12	91.12	101.82	Tie to	1076A-11H-1, 125	91.56	101.82
1076A-11H-6, 52	98.05	108.31	Tie to	1076D-11H-3, 6.5	97.57	108.31
1076D-11H-6, 96	102.96	113.70	Tie to	1076A-12H-2, 100	102.30	113.70
1076A-12H-4, 112	105.42	116.82	Tie to	1076D-12H-1, 65	104.66	116.82
1076D-12H-6, 56	112.06	124.22	Tie to	1076C-13H-3, 124	112.34	124.22
1076C-13H-6, 84	116.44	128.32	Tie to	1076A-13H-6, 34	116.06	128.32
1076A-13H-7, 52	117.72	129.98	Tie to	1076C-14H-2, 42	118.24	129.98
1076C-14H-8, 84	127.64	139.38				

Note: The tie points are listed in standard ODP meters below seafloor (mbsf) and meters composite depth (mcd).

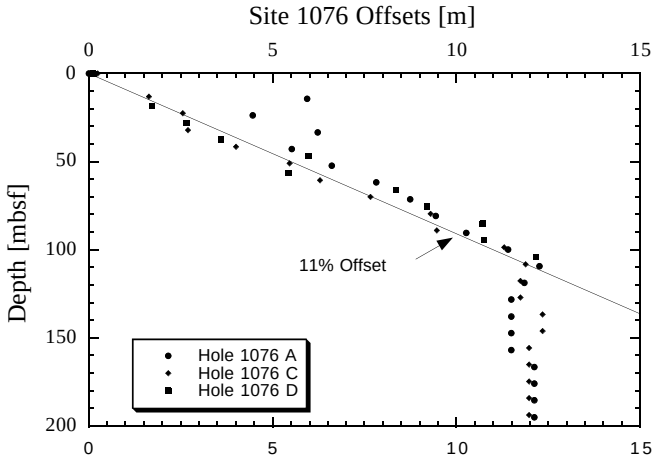

Figure 16. Core offsets applied to Site 1076 plotted against standard ODP meters below seafloor (mbsf). A linear 11% growth of meters composite depth (mcd) compared with mbsf is indicated by an arrow.

values of ~1535 m/s between 35 and 70 mbsf (Fig. 24B, C). No velocities from discrete measurements could be determined below 70 mbsf because of high signal attenuation. The general trend of discrete velocities is similar to wet bulk density and GRAPE profiles in the depth range between 0 and 70 mbsf (Fig. 25).

Index Properties

Results of wet bulk density, porosity, and moisture content are presented in Figures 27A, 27B, and 27C, respectively (also see Table 14 on CD-ROM, back pocket, this volume). Density and porosity show a negative correlation, whereas moisture content is parallel to the porosity profile. In general, density values vary only gradually, with an overall increase from 1350 to 1450 kg/m^3, revealing a homogenous composition of the sediment (see "Lithostratigraphy" section, this chapter). The overall trend to higher values is caused primarily by compaction. Porosity decreases from 85% in the top section to 70% at 200 mbsf, which results from dewatering of the clay-rich sediments.

Thermal Conductivity and Geothermal Gradient

The thermal conductivity profile for Hole 1076A was obtained with the single-probe insertion method in every second core section (see "Explanatory Notes" chapter, this volume). The values display a significant overall scatter throughout the hole (Fig. 26B). Undetected void spaces within the sediment may have deteriorated the measurements. In some intervals, thermal conductivity seems to follow the undrained vane shear strength profile (Fig. 26C).

In Hole 1076A, the Adara tool was deployed to measure formation temperature. A preliminary analysis provided three data points, which were used to estimate a geothermal gradient of 45°C/km, but further analyses will be required to confirm this result.

Vane Shear Strength

An undrained vane-shear measurement was performed in the bottom part of each core section. Local minima and maxima of shear strength within each core are related to the differential stress of gas expansion, which acts mainly on the top and bottom sections of each core. Figure 26C shows the undrained vane-shear profile. The profile shows an overall increase of shear strength values down to ~170 mbsf (Fig. 26C). Below 115 mbsf, scatter increases and maximum values vary significantly for each core. It is unclear which of the vane-shear measurements represent undisturbed sediments.

REFERENCES

Bé, A.W.H., and Tolderlund, D.S., 1971. Distribution and ecology of living planktonic foraminifera in surface waters of the Atlantic and Indian Oceans. *In* Funnel, B.M., and Riedel, W.R. (Eds.), *The Micropaleontology of Oceans:* Cambridge (Cambridge Univ. Press), 105–149.

Berggren, W.A., Kent, D.V., Swisher, C.C., III, and Aubry, M.-P., 1995. A revised Cenozoic geochronology and chronostratigraphy. *In* Berggren, W.A., Kent, D.V., Aubry, M.-P., and Hardenbol, J. (Eds.), *Geochronology, Time Scales and Global Stratigraphic Correlation.* Spec. Publ.—Soc. Econ. Paleontol. Mineral. (Soc. Sediment. Geol.), 54:129–212.

Boersma, A., 1984a. Oligocene and other Tertiary benthic foraminifers from a depth traverse down Walvis Ridge, Deep Sea Drilling Project Leg 74, Southeast Atlantic. *In* Hay, W.W., Sibuet, J.-C., et al., *Init. Repts. DSDP,* 75: Washington (U.S. Govt. Printing Office), 1273–1300.

————, 1984b. Pliocene planktonic and benthic foraminifers from the southeastern Atlantic Angola margin: Leg 75, Site 532, Deep Sea Drilling Project. *In* Hay, W.W., Sibuet, J.-C., et al., *Init. Repts. DSDP, 75 (Pt. 2):* Washington (U.S. Govt. Printing Office), 657–670.

Claypool, G.E., and Kvenvolden, K.A., 1983. Methane and other hydrocarbon gases in marine sediment. *Annu. Rev. Earth Planet. Sci.,* 11:299–327.

Emerson, S., and Hedges, J.I., 1988. Processes controlling the organic carbon content of open ocean sediments. *Paleoceanography,* 3:621–634.

Gartner, S., 1977. Calcareous nannofossil biostratigraphy and revised zonation of the Pleistocene. *Mar. Micropaleontol.,* 2:1–25.

Imbrie, J., Hays, J.D., Martinson, D.G., McIntyre, A., Mix, A.C., Morley, J.J., Pisias, N.G., Prell, W.L., and Shackleton, N.J., 1984. The orbital theory of Pleistocene climate: support from a revised chronology of the marine $\delta^{18}O$ record. *In* Berger, A., Imbrie, J., Hays, J., Kukla, G., and Saltzman, B. (Eds.), *Milankovitch and Climate* (Pt. 1), NATO ASI Ser. C, Math Phys. Sci., 126:269–305.

Jansen, J.H.F., Alderliesten, C., Houston, C.M., De Jong, A.F.M., Van der Borg, K., and Van Iperen, J.M., 1989. Aridity in equatorial Africa during the last 225,000 years: a record of opal phytoliths/freshwater diatoms from the Zaire (Congo) deep-sea fan (northeast Angola basin). *Radiocarbon,* 31:557–569.

Jonkers, H.A., 1984. Pliocene benthonic foraminifera from homogeneous and laminated marls on Crete. *Utrecht Micropaleontol. Bull., I.G.C.P. Proj. No. 1,* 31:1–179.

Locker, S., 1996. Cenozoic siliceous flagellates from the Fram Strait and the East Greenland Margin: biostratigraphic and paleoceanographic results. *In* Thiede, J., Myhre, A.M., Firth, J.V., Johnson, G.L., and Ruddiman, W.F. (Eds.), *Proc. ODP, Sci. Results,* 151: College Station, TX (Ocean Drilling Program), 101–124.

Martini, E., 1971. Standard Tertiary and Quaternary calcareous nannoplankton zonation. *In* Farinacci, A. (Ed.), *Proc. 2nd Int. Conf. Planktonic Microfossils Roma:* Rome (Ed. Tecnosci.), 2:739–785.

McIver, R.D., 1975. Hydrocarbon occurrences from JOIDES Deep Sea Drilling Project. *Proc. Ninth Petrol. Congr.,* 269–280.

Meyers, P.A., 1994. Preservation of elemental and isotopic source identification of sedimentary organic matter. *Chem. Geol.,* 144:289–302.

————, 1997. Organic geochemical proxies of paleoceanographic, paleolimnologic, and paleoclimatic processes. *Org. Geochem.,* 27:213–250.

Millero, F.J., and Sohn, M.L., 1992. *Chemical Oceanography:* Boca Raton (CRC Press).

Mix, A.C., Rugh, W., Pisias, N.G., Veirs, S., Leg 138 Shipboard Sedimentologists (Hagelberg, T., Hovan, S., Kemp, A., Leinen, M., Levitan, M., Ravelo, C.), and Leg 138 Scientific Party, 1992. Color reflectance spectroscopy: a tool for rapid characterization of deep-sea sediments. *In* Mayer, L., Pisias, N., Janecek, T., et al., *Proc. ODP, Init. Repts.,* 138 (Pt. 1): College Station, TX (Ocean Drilling Program), 67–77.

Moore, T.C., Jr., 1995. Radiolarian stratigraphy, Leg 138. *In* Pisias, N.G., Mayer, L.A., Janecek, T.R., Palmer-Julson, A., and van Andel, T.H. (Eds.), *Proc. ODP, Sci. Results,* 138: College Station, TX (Ocean Drilling Program), 191–232.

Okada, H., and Bukry, D., 1980. Supplementary modification and introduction of code numbers to the low-latitude coccolith biostratigraphic zonation (Bukry, 1973; 1975). *Mar. Micropaleontol.,* 5:321–325.

Peters, K.E., 1986. Guidelines for evaluating petroleum source rock using programmed pyrolysis. *AAPG Bull.,* 70:318–329.

Singer, A., 1984. The paleoclimatic interpretation of clay minerals in sediments: a review. *Earth-Sci. Rev.,* 21:251–293.

Tric, E., Laj, C., Valet, J.-P., Tucholka, P., Paterne, M., and Guichard, F., 1991. The Blake geomagnetic event: transition geometry, dynamical characteristics and geomagnetic significance. *Earth Planet. Sci. Lett.,* 102:1–13.

Tucholka, P., Fontugue, M., Guichard, F., and Paterne, M., 1987. The Blake polarity episode in cores from the Mediterranean Sea. *Earth Planet. Sci. Lett.,* 86:320–326.

Ufkes, E., Jansen, J.H.F., Brummer, G.-J.A., in press. Living planktonic foraminifera in the Eastern South Atlantic during spring: indicators of water masses, upwelling and the Congo (Zaire) river plume. *Mar. Micropaleontol.*

van der Gaast, S.J., and Jansen, J.H.F., 1984. Mineralogy, opal, and manganese of Middle and Late Quaternary sediments of the Zaire (Congo) deep-sea fan: origin and climatic variation. *Neth. J. Sea Res.,* 17:313–341.

Van der Zwaan, G.J., 1982. Paleoecology of Late Miocene Mediterranean foraminifera. *Utrecht Micropaleontol. Bull.,* 25:202.

Weaver, P.P.E., 1993. High resolution stratigraphy of marine Quaternary sequences. *In* Hailwood, E.A., and Kidd, R.B. (Eds.), *High Resolution Stratigraphy.* Geol. Soc. Spec. Publ. London, 70:137–153.

Ms 175IR-104

NOTE: Core-description forms ("barrel sheets") and core photographs can be found in Section 4, beginning on page 581. Forms containing smear-slide data can be found on CD-ROM. See Table of Contents for materials contained on CD-ROM.

Table 10. Interstitial water composition for Hole 1076A.

Core, section, interval (cm)	Depth (mbsf)	pH	Alkalinity (mM)	Salinity	Cl^- (titr) (mM)	Cl^- (IC) (mM)	SO_4^{2-} (mM)	Na^+ (mM)	Mg^{2+} (mM)	Ca^{2+} (mM)	K^+ (mM)	H_4SiO_4 (mM)	NH_4^+ (μM)	PO_4^{3-} (μM)	Sr^{2+} (μM)
175-1076A-															
1H-1, 140-150	1.40	7.58	6.778	35.0	555	552	25.90	479	51.25	9.99	12.28	508	613	36	90
1H-3, 140-150	4.40	7.72	13.025	35.0	555	548	20.11	478	49.92	8.86	12.66	645	1130	63	90
2H-2, 140-150	7.70	7.74	24.119	34.5	556	554	11.54	479	48.60	7.46	12.17	649	1771	100	88
3H-3, 140-150	18.70	7.78	34.049	34.5	559	554	1.70	481	46.32	5.65	12.22	641	2288	108	90
4H-3, 140-150	28.20	7.81	35.062	34.0	561	563	0.10	483	45.59	4.84	12.06	699	2467	109	95
5H-3, 140-150	37.70	7.79	35.728	34.0	562	571	0.43	488	45.36	4.28	11.78	703	2529	94	99
6H-3, 140-150	47.20	7.78	36.188	34.0	562	572	0.00	485	45.91	4.41	12.49	784	2673	94	101
7H-3, 140-150	56.70	7.76	35.938	34.5	563	569	0.00	487	45.41	4.21	12.67	801	3018	74	100
8H-3, 140-150	66.20	7.60	35.921	34.0	565	565	0.00	491	43.84	4.61	12.76	736	3335	92	99
9H-3, 140-150	75.70	7.19	35.126	34.0	567	570	0.00	494	42.62	4.76	13.31	805	3707	102	98
10H-3, 130-140	85.10	7.86	33.597	34.5	568	575	0.00	499	40.31	4.38	13.54	775	4141	95	97
11H-3, 120-130	94.50	7.83	31.046	34.0	569	566	0.00	498	39.47	4.37	13.44	712	4520	78	94
14H-3, 130-150	123.10	7.72	20.849	33.5	568	586	0.04	499	33.91	3.45	14.74	701	6112	42	92
17H-3, 140-150	150.65	7.44	20.260	33.0	569	570	0.00	509	29.67	3.24	14.14	994	7212	50	99
20H-2, 140-150	178.70	7.56	22.280	33.5	575	574	0.00	518	28.13	4.38	15.04	842	7942	29	104
22H-5, 140-150	202.20	7.46	33.271	34.0	578	600	0.98	534	26.13	4.97	16.36	890	9217	33	114

Note: Cl^- (titr) = analyzed by titration and Cl^- (IC) = analyzed by ion chronatography.

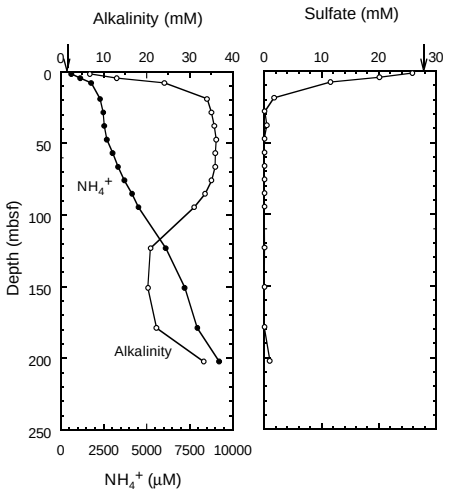

Figure 17. Downcore profiles of dissolved alkalinity, sulfate, and ammonium at Hole 1076A. Arrows = mean ocean-bottom-water values taken from Millero and Sohn (1992).

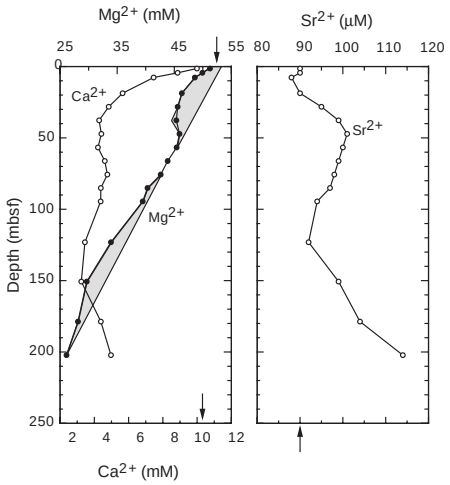

Figure 18. Downcore profiles of Ca^{2+}, Mg^{2+}, and Sr^{2+} at Hole 1076A. Shaded region associated with Mg^{2+} profile indicates additional removal of Mg^{2+}, which may reflect dolomite formation. Arrows = mean ocean-bottom-water values taken from Millero and Sohn (1992).

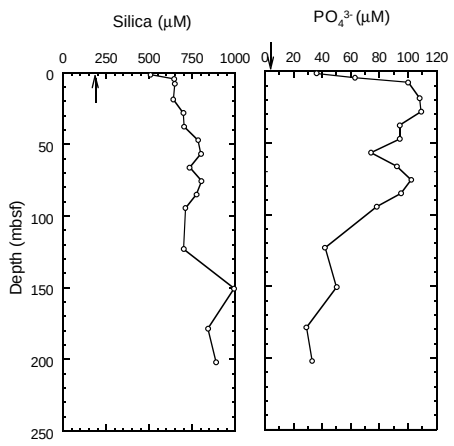

Figure 19. Downcore profiles of dissolved silica and phosphate at Hole 1076A. Arrows = mean ocean-bottom-water values taken from Millero and Sohn (1992).

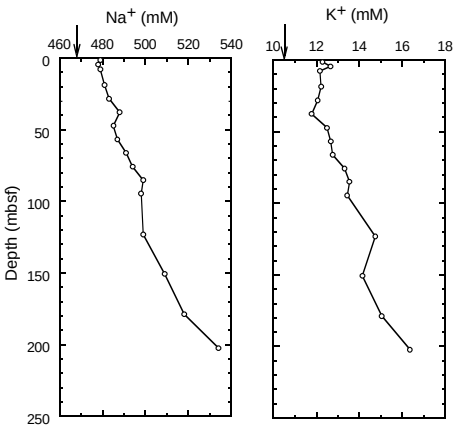

Figure 20. Downcore profiles of dissolved Na^{+} and K^{+} at Hole 1076A. Arrows = mean ocean-bottom-water values taken from Millero and Sohn (1992).

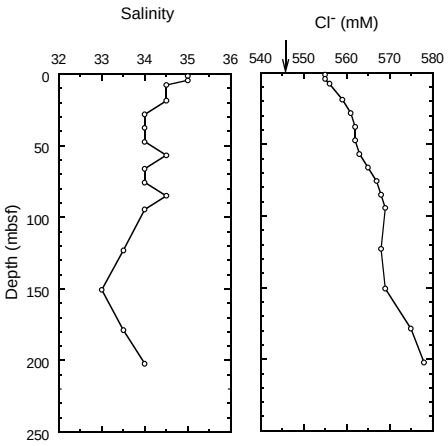

Figure 21. Downcore profiles of salinity and dissolved Cl^{-} at Hole 1076A. Arrow = mean ocean-bottom-water values taken from Millero and Sohn (1992).

Table 11. Percentages of inorganic and total carbon, total nitrogen, and total sulfur in sediment samples from Hole 1076A.

Core, section, interval (cm)	Depth (mbsf)	IC (wt%)	$CaCO_3$ (wt%)	TC (wt%)	TOC (wt%)	TN (wt%)	TS (wt%)	C/N (atomic)
175-1076A-								
1H-3, 47-48	3.47	0.49	4.12	1.42	0.93	0.24	1.29	4.5
2H-1, 46-47	5.26	0.46	3.91	3.17	2.70	0.26	1.82	12.2
2H-3, 46-47	8.26	0.52	4.37	3.68	3.15	0.26	1.83	14.2
2H-5, 46-47	11.26	0.33	2.80					
3H-1, 46-47	14.76	0.28	2.34	2.76	2.48	0.21	1.62	13.8
3H-3, 46-47	17.76	0.16	1.39	2.51	2.35	0.19	2.76	14.5
3H-5, 46-47	20.76	0.10	0.91					
4H-1, 46-47	24.26	1.34	11.21	4.20	2.85	0.21	2.60	15.9
4H-3, 46-47	27.26	1.08	9.02	3.27	2.19	0.18	3.44	14.2
4H-5, 46-47	30.26	1.55	12.92					
5H-1, 46-47	33.76	0.09	0.82	2.74	2.64	0.19	2.15	16.3
5H-3, 46-47	36.76	0.11	0.91	3.99	3.88	0.32	3.28	14.2
5H-5, 46-47	39.76	0.52	4.37					
6H-3, 46-47	46.26	0.46	3.87	3.65	3.19	0.24	3.22	15.6
6H-5, 46-47	49.26	0.44	3.73					
7H-1, 46-47	52.76	0.18	1.53	4.44	4.26	0.33	3.03	15.1
7H-3, 46-47	55.76	1.44	12.04	3.25	1.80	0.16	4.28	13.2
7H-5, 46-47	58.76	0.80	6.67					
8H-1, 46-47	62.26	0.25	2.10					
8H-3, 46-47	65.26	0.09	0.80	2.64	2.55	0.20	1.82	14.9
8H-5, 46-47	68.31	0.03	0.26					
9H-1, 46-47	71.76	0.11	0.97	2.62	2.51	0.23	2.12	12.8
9H-3, 46-47	74.76	1.94	16.16	4.34	2.40	0.17	2.52	16.5
9H-5, 46-47	77.58	0.68	5.71					
10H-1, 46-47	81.26	0.16	1.40	2.52	2.35	0.16	2.26	17.2
10H-3, 46-47	84.26	0.12	1.06	2.91	2.78	0.22	2.44	14.8
10H-5, 46-47	87.16	0.07	0.64					
11H-1, 46-47	90.76	0.12	1.05	2.54	2.41	0.18	3.25	15.7
11H-3, 46-47	93.76	0.34	2.84	3.01	2.67	0.20	1.85	15.6
11H-5, 46-47	96.49	0.09	0.83					
12H-1, 46-47	100.26	0.27	2.27	2.24	1.96	0.16	2.39	14.3
12H-3, 46-47	103.26	0.14	1.18	2.68	2.54	0.20	1.77	14.9
12H-5, 46-47	106.26	0.09	0.82					
13H-3, 46-47	111.66	0.44	3.71	3.02	2.57	0.20	2.61	15.0
13H-5, 46-47	114.66	0.38	3.24					
14H-1, 46-47	119.26	0.70	5.87	3.35	2.65	0.22	2.46	14.1
14H-3, 46-47	122.26	0.31	2.58	2.60	2.29	0.20	2.18	13.4
14H-5, 46-47	125.23	1.61	13.45					
15H-1, 52-53	128.82	0.71	5.94	2.88	2.17	0.18	3.29	14.1
15H-3, 46-47	131.81	0.43	3.64					
15H-5, 46-47	134.83	0.53	4.43	2.91	2.38	0.22	2.02	12.7
16H-1, 46-47	138.26	1.55	12.94	3.86	2.30	0.20	1.64	13.5
16H-3, 46-47	141.26	0.40	3.40	2.99	2.59	0.21	2.05	14.4
16H-5, 46-47	144.26	0.43	3.65					
17H-2, 46-47	148.21	0.28	2.35	4.60	4.32	0.32	2.56	15.8
17H-4, 46-47	151.21	0.20	1.71	2.01	1.81	0.18	2.50	11.8
17H-6, 46-47	154.21	0.09	0.75					
18H-1, 46-47	157.26	0.20	1.69	2.38	2.17	0.19	2.70	13.4
18H-3, 46-47	160.26	0.30	2.55	3.06	2.76	0.22	1.57	14.7
18H-5, 46-47	163.26	0.23	1.91					
19H-1, 46-47	166.76	0.26	2.19	3.56	3.29	0.27	2.79	14.3
19H-3, 46-47	169.76	0.42	3.53	2.54	2.12	0.19	3.20	12.8
19H-5, 46-47	172.76	0.23	1.99					
20H-1, 46-47	176.26	0.40	3.35	2.53	2.13	0.20	2.64	12.2
20H-3, 46-47	179.26	0.24	2.01	2.04	1.80	0.17	1.95	12.5
20H-5, 46-47	182.26	0.46	3.90					
21H-3, 46-47	187.70	0.33	2.81	2.80	2.46	0.22	1.77	13.1
21H-5, 46-47	190.70	0.22	1.91	2.73	2.50	0.24	2.83	12.5
22H-1, 46-47	195.26	0.23	1.95					
22H-3, 46-47	198.26	0.40	3.37	3.58	3.17	0.28	2.50	13.4
22H-5, 46-47	201.26	0.25	2.13	2.41	2.16	0.19	2.47	13.0

Notes: IC = inorganic carbon; $CaCO_3$ = calcium carbonate; TC = total carbon; TOC = total organic carbon; TN = total nitrogen; TS = total sulfur; and C/N = carbon/nitrogen ratio. TOC concentrations are calculated from the difference between IC and TC concentrations. C/N ratios are calculated from TOC and TN concentrations and are given as atom/atom ratios.

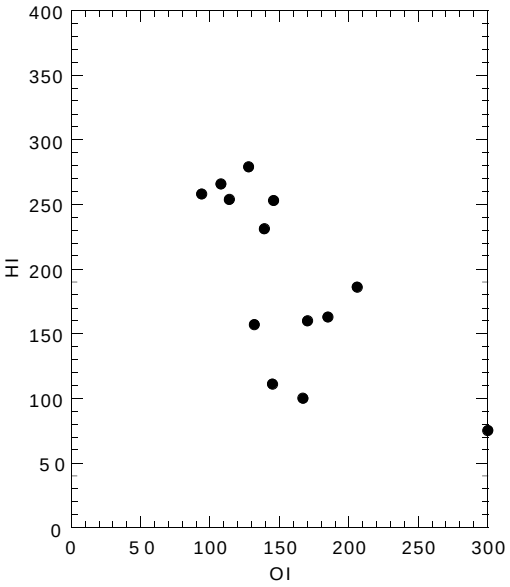

Figure 22. Rock-Eval Van Krevelen–type diagram of sediments from Hole 1076A. Organic matter appears to be a mixture of type II algal material that has been variably oxidized and type III continental or detrital organic matter. HI = milligrams of hydrocarbons per gram of organic carbon; OI = milligrams of CO_2 per gram of organic carbon.

Table 12. Results of Rock-Eval pyrolysis analyses of sediments from Hole 1076A.

Core, section, interval (cm)	Depth (mbsf)	TOC (wt%)	S_1	S_2	S_3	T_{max} (°C)	HI	OI
175-1076A-								
2H-3, 46-47	8.26	3.16	0.66	4.98	4.20	412	157	132
4H-1, 46-47	24.26	2.85	0.38	3.19	4.16	429	111	145
5H-3, 46-47	36.76	3.88	0.74	10.04	3.67	420	258	94
7H-1, 46-47	52.76	4.26	0.78	10.84	4.88	419	254	114
7H-3, 46-47	55.76	1.80	0.16	1.35	5.41	414	75	300
9H-1, 46-47	71.76	2.50	0.32	6.34	3.67	466	253	146
10H-3, 46-47	84.26	2.78	0.18	2.79	4.67	467	100	167
14H-1, 46-47	119.26	2.65	0.47	4.25	4.51	416	160	170
15H-3, 46-47	131.81	2.38	0.31	3.89	4.41	418	163	185
17H-2, 46-47	148.21	4.32	0.72	11.51	4.69	417	266	108
19H-1, 46-47	166.76	3.30	0.59	7.65	4.61	416	231	139
20H-3, 46-47	179.26	1.80	0.19	3.35	3.72	467	186	206
22H-3, 46-47	198.26	3.17	1.00	8.87	4.08	406	279	128

Notes: TOC = total organic carbon; HI = hydrogen index; and OI = oxygen index. Units of the various Rock-Eval parameters are given in the "Organic Geochemistry" section of the "Explanatory Notes" chapter (this volume).

Table 13. Results of headspace gas analyses of sediments from Hole 1076A.

Core, section, interval (cm)	Depth (mbsf)	C_1 (ppmv)	CO_2 (ppmv)	C_2= (ppmv)	C_2 (ppmv)	C_3 (ppmv)	C_1/C_2
175-1076A-							
1H-2, 0-5	1.50	2					
2H-3, 0-5	7.80	2	12,288				
3H-4, 0-5	18.80	3					
4H-4, 0-5	28.30	2,055			0.4		5,138
5H-4, 0-5	37.80	25,623			3.3		7,765
6H-4, 0-5	47.30	37,251		0.2	5.0	0.3	7,450
7H-4, 0-5	56.80	47,483	22,727	0.3	7.6		6,248
8H-4, 0-5	66.30	69,413		0.4	11.0		6,310
9H-4, 0-5	75.82	32,313		0.3	7.6	1.2	4,252
10H-4, 0-5	85.20	25,922		0.2	5.9	1.2	4,394
11H-4, 0-5	94.70	34,361		0.4	9.8	2.1	3,506
12H-1, 0-5	99.80	26,174	9,233	0.3	7.1	1.4	3,686
13H-8, 0-5	118.70	8,967		0.3	3.4	0.8	2,637
14H-4, 0-5	123.30	22,345		0.4	9.8	2.8	2,280
15H-7, 0-5	137.37	10,637		0.2	5.1	1.9	2,086
16H-7, 0-5	146.80	14,768		0.5	7.3	3.1	2,023
17H-4, 0-5	150.75	13,694	8,751	0.3	8.3	3.6	1,650
18H-7, 0-5	165.80	15,642		0.3	8.2	3.6	1,908
19H-6, 145-150	175.25	13,017		0.3	8.0	4.0	1,627
20H-3, 0-5	178.80	11,441		0.3	8.0	4.5	1,430
21H-7, 0-5	193.24	8,936		0.1	5.5	2.5	1,625
22H-6, 0-5	202.30	12,579	25,260	0.5	8.5	5.3	1,480

Notes: C_1 = methane; CO_2 = carbon dioxide; C_2= = ethene; C_2 = ethane; and C_3 = propane. Dominance of C_1 over C_2 indicates that the gases originate from in situ microbial degradation of organic matter.

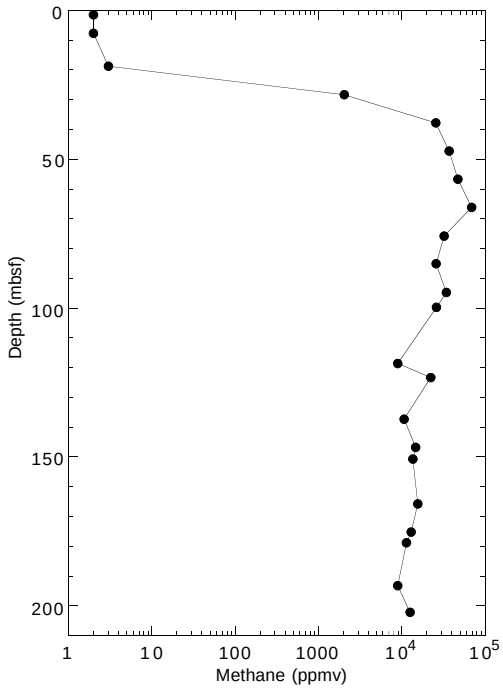

Figure 23. Headspace methane concentrations in sediments from Hole 1076A.

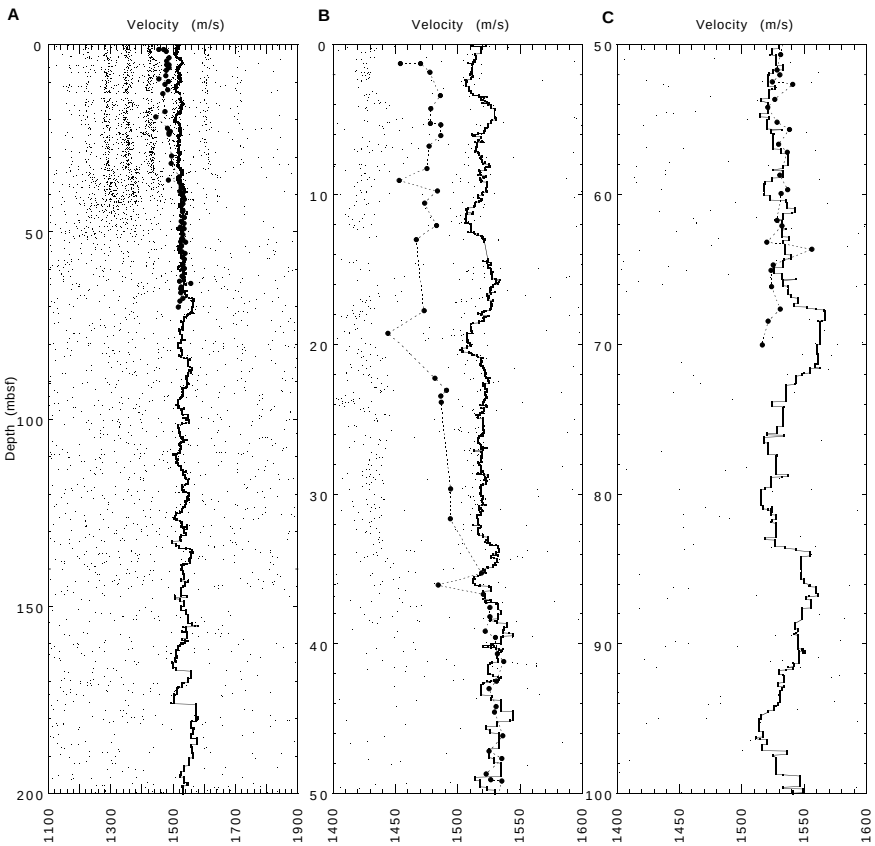

Figure 24. Plots of (**A**) ultrasonic compressional velocities from the MST (dots) and filtered velocity log (solid line) compared with discrete velocities at (**B**) 0–50 mbsf and (**C**) 50–100 mbsf for Hole 1076A.

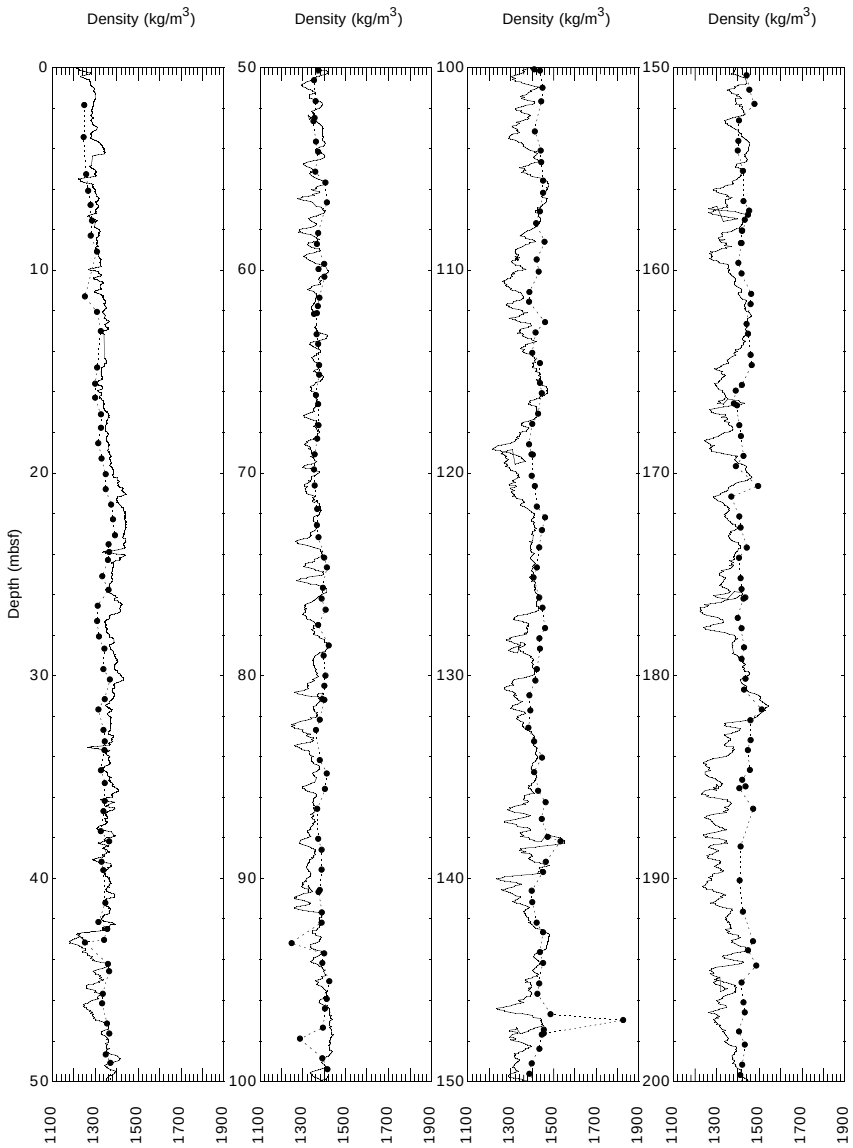

Figure 25. Near-continuous filtered and smoothed GRAPE profile (solid line) from the MST compared with wet bulk density (solid circles) obtained from index properties measurements for Hole 1076A.

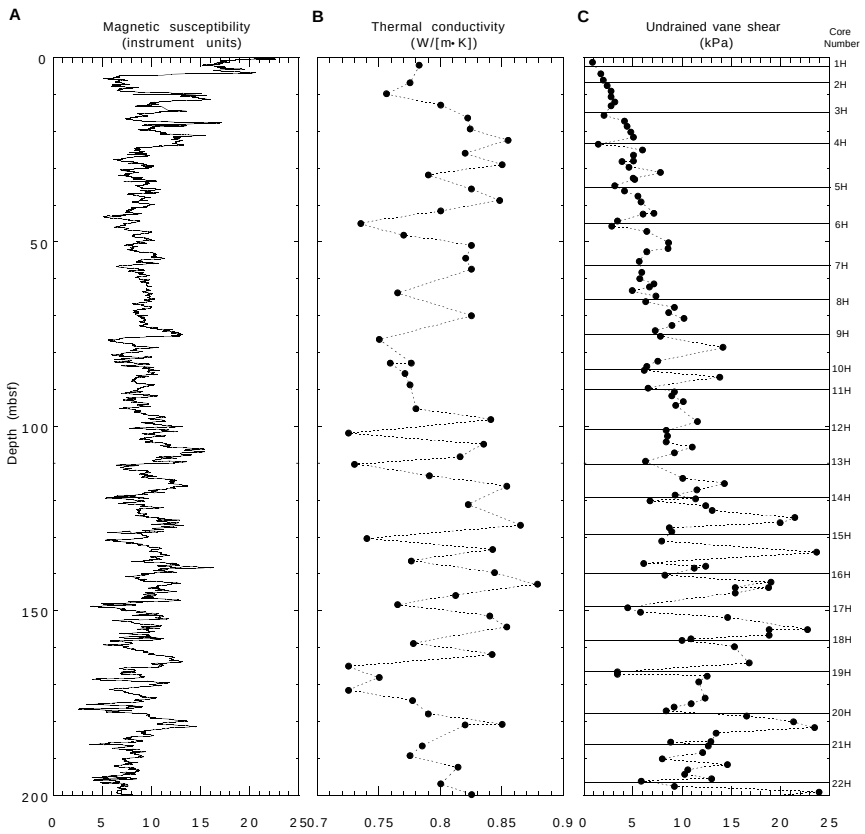

Figure 26. Plots of (**A**) near-continuous magnetic susceptibility from the MST compared with (**B**) thermal conductivity and (**C**) undrained vane-shear measurements for Hole 1076A.

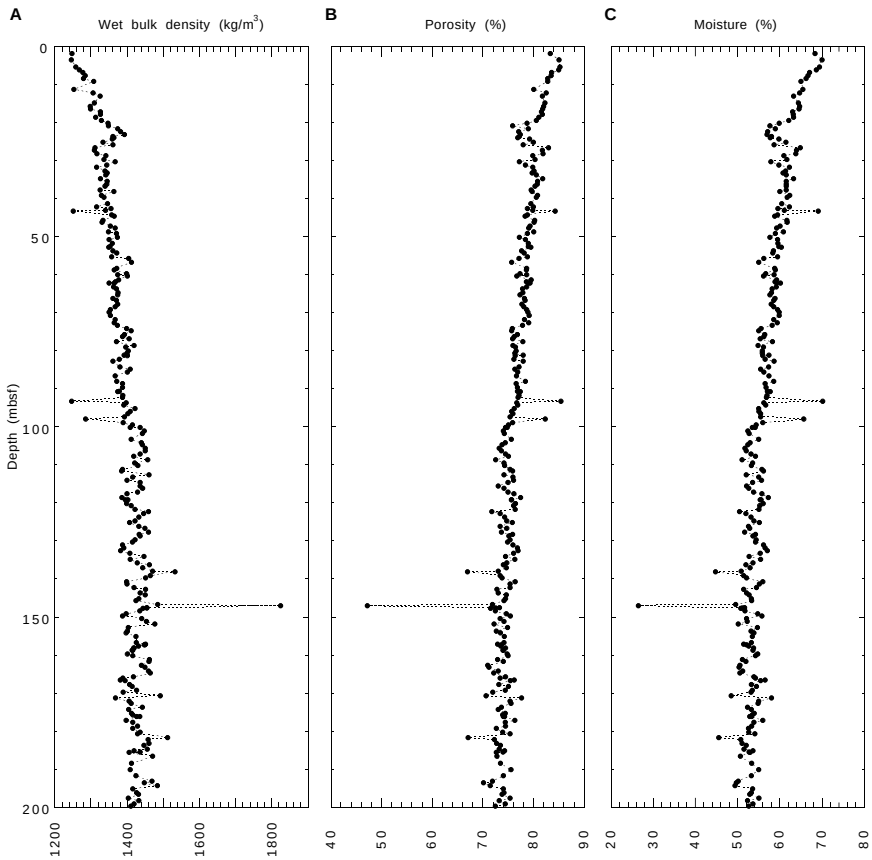

Figure 27. Plots of (**A**) wet bulk density, (**B**) porosity, and (**C**) moisture content derived from index properties measurements for Hole 1076A.